AGU ADVANCING EARTH AND SPACE SCIENCES

Water Resources Research

RESEARCH ARTICLE
10.1029/2024WR038968

Hydrodynamics of Four Moments in the Life of a Floodplain Forest in Compound Channels

Luiz E. D. de Oliveira[1,2,3,4], **Johannes G. Janzen**[2], **Frederik Folke**[4,5], **Florian Wittmann**[6], **Nils P. Huber**[4], **Mário J. Franca**[3], **and Carlo Gualtieri**[1,7]

[1]Department of Civil, Building and Environmental Engineering (DICEA), University of Naples Federico II (UNINA), Napoli, Italy, [2]Federal University of Mato Grosso do Sul (UFMS), Campo Grande, Brazil, [3]Institute for Water and Environment (IWU), Karlsruhe Institute of Technology (KIT), Karlsruhe, Germany, [4]Federal Waterways Engineering and Research Institute (BAW), Karlsruhe, Germany, [5]Ostbayerische Technische Hochschule Regensburg (OTH Regensburg), Regensburg, Germany, [6]Department of River and Wetland Ecology, Institute of Geography and Geoecology (IFGG), Karlsruhe Institute of Technology (KIT), Karlsruhe, Germany, [7]Department of Structures for Engineering and Architecture (DIST), University of Naples Federico II (UNINA), Napoli, Italy

Key Points:

- Floodplain forest aging must be considered in river management as it considerably alters the hydrodynamics of floods in compound channels
- A model was developed to describe the mean flow profile under the influence of local effects caused by vegetation
- A conceptual model of the flow in a compound channel with vegetated floodplain and its consequences to the mixing layer was proposed

Supporting Information:

Supporting Information may be found in the online version of this article.

Correspondence to:

L. E. D. de Oliveira,
luiz.oliveira@kit.edu

Citation:

de Oliveira, L. E. D., Janzen, J. G., Folke, F., Wittmann, F., Huber, N. P., Franca, M. J., & Gualtieri, C. (2026). Hydrodynamics of four moments in the life of a floodplain forest in compound channels. *Water Resources Research*, *62*, e2024WR038968. https://doi.org/10.1029/2024WR038968

Received 20 SEP 2024
Accepted 10 FEB 2026

Abstract Natural rivers often function as compound channels, comprising main channel and floodplain. Flow dynamics in these systems, particularly during floods, are influenced by factors such as vegetation, and flood intensity. Floodplain vegetation significantly modifies flow structures, affecting hydraulic conveyance and ecological functions. As floodplain forests develop through succession, their composition and hydraulic characteristics evolve, altering the flow in compound channels. This study examines the impact of forest succession, forest management and flood intensity on compound channel hydrodynamics. The forest composition was based on a forest in the Upper Rhine, and was heterogeneously distributed through the experimental flume. Our results revealed that forest aging reduces, due to the reduction in the leaf area index (LAI), velocity differences and shear, narrowing the mixing layer. Consequently, lateral mass exchanges decreased and a hydraulically smoother and more uniform flow was created in the floodplain, with implications for hydraulic modeling. Forest management practices, such as selective vegetation removal, can significantly alter flow hydrodynamics, particularly water depth. Flood intensity influences the peak mean transverse velocity, backwater effect, and lateral discharge distribution. Solute dispersion remains mainly advective in the main channel, with flood intensity exerting limited influence. In contrast, vegetation enhances tracer dispersion within the floodplain and at the channel–floodplain interface. The study highlights the limitations of traditional analytical models and emphasizes the need for approaches that incorporate natural vegetation distribution, such as the one developed here. These findings underscore the importance of integrating forest succession into river management to maintain flood protection and navigability.

Plain Language Summary Rivers are often divided in two parts: a main channel where water flows most of the year and a floodplain that is covered with water during floods. Vegetation in these floodplains plays a crucial role in river flow patterns and ecosystem health. As forests in the floodplains age, their structure changes, affecting how water flows through the river system. This study investigated how forest growth, forest management, and flood intensity impact water flow. In our study, the forest composition was inspired by a floodplain forest in the Upper Rhine. We found that as floodplain forests age, the differences in water flow velocity between the main channel and the floodplain become smaller. These changes affect how water and materials mix and move between the two areas. Altogether, this influences how river flow is represented in hydraulic models. Managing these forests, for instance by selectively removing some trees, can help control these effects and protect river dwellers against floods. This type of management can reduce the height of floodwaters upstream and make the river safer for nearby communities. Understanding these changes is important for maintaining the river's health and ensuring it can continue to support both human and ecological needs.

1. Introduction

Rivers are often classified as compound channels, characterized by a vertically segregated main channel (MC), which carries more frequent discharges, and floodplain (FP), inundated during flood events. During floods, the flow extension into both regions leads to crucial mixing processes that play a significant role in shaping the

riverine ecosystem. The overbank flow in compound channels (CC) depends on various geometric and dynamic characteristics that affect the interactions between floodplain and main channel (Dupuis et al., 2017a, 2023; Juez et al., 2019; Nezu et al., 1999; Proust & Nikora, 2020; Stocchino & Brocchini, 2010; Västilä & Jilbert, 2025).

Vegetation significantly impacts the flow structure and conveyance in compound channels (Azevedo et al., 2012; Dupuis et al., 2017a, 2017b; Fernandes et al., 2018; Nagy et al., 2018). For deep flows, vegetation wakes induce three-dimensional vortices that differ the classic quasi-2D behavior in compound channel flows (Azevedo et al., 2012). These authors indicate that the vegetation wake influences both the free surface and near bottom regions in terms of integral length scale, which may have implications for the stresses. For shallow flows, meadow vegetation reduces the conveyed water and the discharge portion in the floodplain Fernandes et al. (2018); Nagy et al. (2018). Furthermore, increased roughness due to the change of vegetation type leads to an increase in water depth, changes in the turbulent structure, and induces mean transverse flow velocities (u_y) (Dupuis et al., 2017a, 2017b; Rominger & Nepf, 2011). The increase in vegetation density has a positive feedback on floodplain roughness and consequently reduces flow conveyance (Nagy et al., 2018), increasing the lateral mass exchange between floodplain and main channel while the flow readjusts (Dupuis et al., 2017a). Additionally, vegetation positioning affects the flow; for instance, in simple channels, randomized vegetation exhibits higher local velocity gradients (Ricardo et al., 2016), promotes the generation of background turbulence (Ricardo et al., 2018) and disrupts the balance between the production and dissipation rates of turbulent kinetic energy (TKE), even though TKE remains smoothly distributed (Ricardo et al., 2014). Moreover, the increase in vegetation density reduces, in heterogeneous spatial vegetation distributions, the bulk drag coefficient in a faster rate than in staggered spatial distributions (Nepf, 1999). In the vertical direction, a heterogeneous submergence distribution increases both turbulent intensities and TKE in the main channel compared to single-layered floodplain vegetation (Barman & Kumar, 2022). Vegetation composition changes with time (Wittmann et al., 2010), affecting hydraulic relevant characteristics such as stiffness, submergence and distribution in the field. Despite recent efforts to characterize vegetated flow in compound channels, the distribution and densities are often arbitrary or based on a uniform grid, conditions not found in natural floodplain forests.

Vegetation in floodplains provides several ecosystem services, including promoting sedimentation and influencing sediment transport (Juez et al., 2019; Lightbody et al., 2019; Västilä & Jilbert, 2025; Villada Arroyave & Crosato, 2010), protecting riverbanks and facilitating the formation of natural levees (Branß et al., 2022; Rominger et al., 2010), and influencing river morphology by encouraging meandering over braiding (Crosato & Saleh, 2011; Rominger et al., 2010). Additionally, floodplain vegetation contributes to soil conservation and enhances the storage of carbon, nitrogen, and phosphorus (Västilä & Jilbert, 2025; Wohl, 2021). Despite these ecological functions, rivers have been altered over the past century to promote inland navigation, resulting in the disconnection of floodplain and main channel. For instance, the Rhine River has been heavily modified over the past two centuries to reduce flood risk and improve navigation, with interventions also addressing public health and geopolitical concerns (Bernhardt, 2000; Ochs et al., 2020).

Those river alterations suppress flow disturbances, disrupting connectivity and ecotones (transition zones between vegetation formations and the non-vegetated environments) between forest patches, consequently reducing habitat heterogeneity and biodiversity (Johnson & Miyanishi, 2007; Nakashizuka, 2001; Ward et al., 1999). This disconnection can also degrade groundwater quality by diminishing the floodplain's ability to filter and store carbon, nitrogen, and phosphorus, leading to higher concentrations of these elements in the water (Trémolières et al., 1997). Restoration projects often aim to restore main channel-floodplain connectivity to enhance habitat abundance and diversity (Wohl, 2021). Among various restoration techniques, managing or reforesting floodplain helps to attenuate peak flows, decrease downstream flood risk, retain dissolved and particulate nutrients and organic matter, and increase floodplain resilience to natural and anthropogenic disturbances (Johnson et al., 2007; Phillips, 2009; Wohl, 2021). However, restoration projects often overlook the impact of forest succession on compound channel systems. Forest aging might also be relevant, particularly in the Upper Rhine, where there are forests that still did not complete secondary succession (Dister et al., 1990), indicating that its characteristics will change as the forest ages. Forest succession and community changes involve vegetation undergoing sequential development from bare surfaces to mature structures (Burrows, 1991; Johnson & Miyanishi, 2007; Nakashizuka, 2001; Ward et al., 1999). There are two successions: (a) primary, which refers to the first colonization of plants and animals, in places where no vegetation was settled before (i.e., new volcanic soils and new deposited sediments) and (b) the secondary succession, in which after a major disturbance event (i.e., intense flood, fire and/or anthropogenic action) there is a reestablishment of organisms (Wittmann et al., 2010).

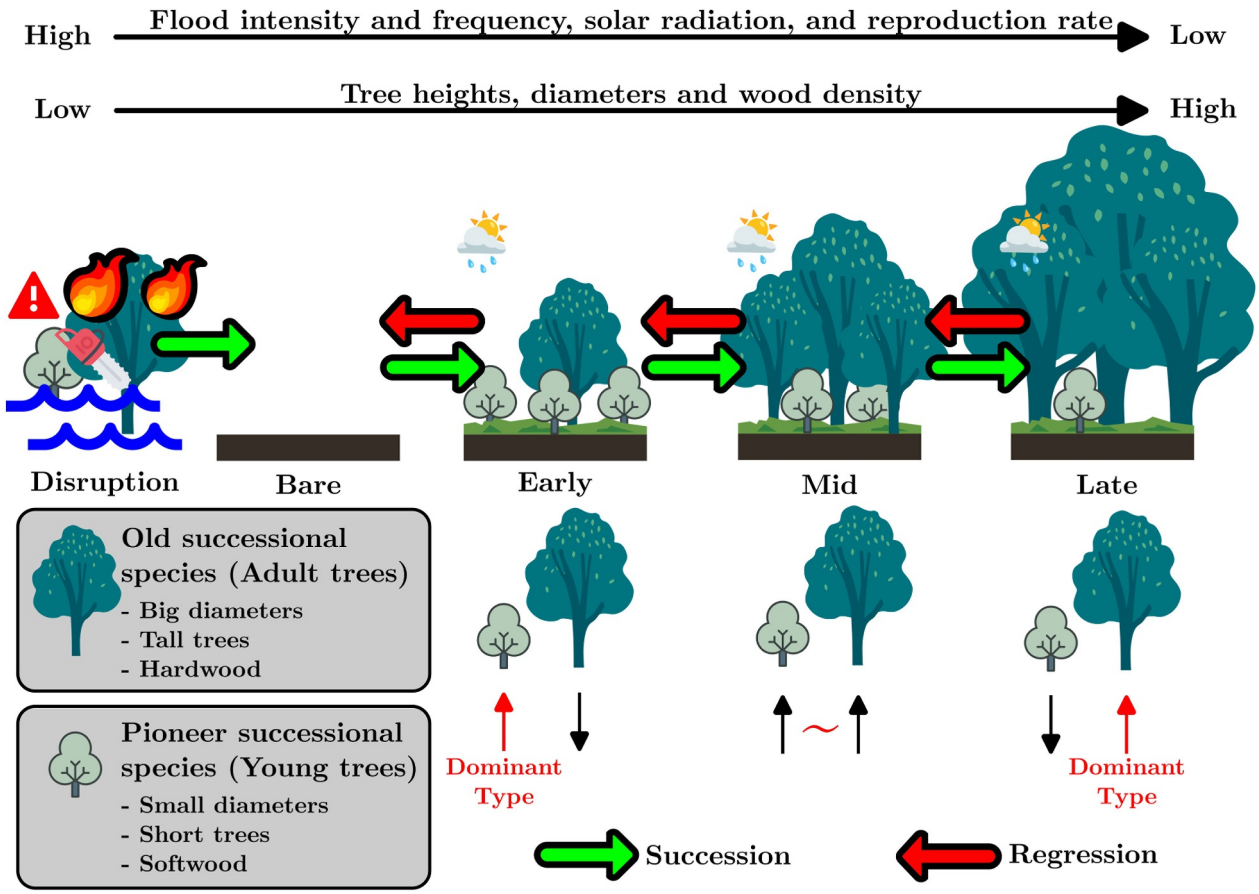

Figure 1. Sketch of the four moments in the life of a forest undergoing a secondary succession, after a disruptive event. The forest succession is not shown as a unidirectional process but allows cycles of succession and regression.

A simple summary of secondary succession in a forest is provided here, with the common structures. Initially, a pioneer community forms from new plants and remnants of previous communities after ecological disturbances (e.g., floods, fires, anthropogenic actions) (Bose et al., 2014; Burrows, 1991). The early stage of forest development is primarily constituted by pioneer tree species (young successional species), which are adapted to pioneer conditions such as full sunlight, high floods, and high levels of disturbance. These species often have a high reproduction rate, short life-cycles, and flexible stems with comparatively low wood specific gravity (softwood) (Wittmann et al., 2022). At this age, flexibility and submergence are the dominant vegetation characteristics, which, in hydraulic terms, result in variable flow resistance as the vegetation undergoes flow-induced reconfiguration (Box et al., 2022). As the forest develops, older successional species appear. These species are adapted to persist even in shaded environments and are characterized by a slower rate of reproduction and rigid stems (hardwood). The mid age forest consists of a mixed distribution of pioneer and older successional species (Burrows, 1991; Egler, 1954). This coexistence creates a double-layered configuration that affects hydraulic roughness, as the drag contribution from leaves (flexible, submerged vegetation) differs from that of stems (rigid, emergent vegetation) (Aberle & Järvelä, 2013; Zhang et al., 2024). As the environment undergoes successional development, there is a progressive dominance of the older successional species over the decades due to competition and changes in the availability of resources such as water, nutrients, and sunlight. Finally, a late or mature stage is achieved, where the forest is mainly composed of older successional species, with higher diameter and basal area, in a dynamic equilibrium (Burrows, 1991; Christensen & Peet, 1984). The stem diameter is directly proportional to the turbulence length scale and turbulence intensity, as stem diameter and spacing together serve as the primary drivers of turbulence in emergent vegetation (Nepf, 2012). Throughout the forest succession, young and adult species coexist, and their presence varies over time and space due to local

disturbances (Nakashizuka, 2001), in a bidirectional process (i.e., succession and regressions) (Burrows, 1991). Figure 1 illustrates the four moments in the life of a forest undergoing a secondary succession.

The relative water depth $H_r = H_{fp}/H_{mc}$ (ratio of the flow depth in the floodplain H_{fp} to that in the main channel H_{mc}) is perhaps the most defining characteristics of the flow structure, being inversely related to the degree of interaction between the floodplain and main channel in compound channels (Ackers, 1993; Nezu et al., 1999; Stocchino & Brocchini, 2010; Tominaga & Nezu, 1991). For sufficiently shallow flows ($H_r < 0.50$), the flow is characterized by the presence of macro-vortices at the interface between the main channel and the floodplain Stocchino and Brocchini (2010) and a monotonic velocity profile across the river section (Dupuis et al., 2017b; Juez et al., 2019; Proust et al., 2017). For deep flows ($H_r > 0.50$), the shear in the transition region is weak, with lower Reynolds shear stresses when compared to shallower conditions (Stocchino & Brocchini, 2010). This shear, defined in terms of the dimensionless shear, $\lambda = (u_{x,mc}^{DA} - u_{x,fp}^{DA})/(u_{x,mc}^{DA} + u_{x,fp}^{DA})$ (where u_x^{DA} is the time- and depth-averaged streamwise velocity, and the subscripts mc and fp refer to the main channel and floodplain, respectively), is related to the presence of coherent structures (Proust et al., 2017). The dimensionless shear significantly impacts the width and structure of the mixing layer (ML) formed between the floodplain and main channel, as well as the maximum values of Reynolds shear stress (Dupuis et al., 2023; Proust et al., 2017, 2022). The introduction of vegetation into the compound channel system increases both H_r and λ due to changes in water depth and velocity (Caroppi et al., 2021; Dupuis et al., 2017b). The transition slope angle reduction has a negative feedback on the intensity and size of secondary velocity components (transverse velocity u_y and vertical velocity u_z) (Xiao et al., 2018), which is also observed in vegetated conditions (Barman & Kumar, 2023). This reduction might impose challenges in the detection or formation of secondary currents, specifically for intermediate flow conditions near to the deep flow limit and deep flows as the reduced topographical influence might lead the secondary currents to negligible magnitudes.

The intensity and direction of the mean transverse flow velocity (u_y^{DA}) influence the discharge distribution between the main channel and floodplain, as well as the mixing layer width, and the dimensionless shear (Dupuis et al., 2017a; Proust et al., 2013, 2017, 2022; Proust & Nikora, 2020). For mean transverse flow directed toward the floodplain, the mixing layer width increases, while the contributions to momentum exchange from mean transverse flow ($-\rho u_x^{DA} u_y^{DA}$, where ρ [kg/m^3] is the water density), turbulent shear stresses ($-\rho\left(\overline{u_x' u_y'}\right)^{DA}$, where u' [m/s] is the velocity fluctuation), and the secondary currents ($-\rho\left[u_x\left(u_y - u_y^{DA}\right)\right]^{DA}$) have similar magnitudes (Proust et al., 2013, 2017; Proust & Nikora, 2020). Conversely, when the mean transverse flow is directed toward the main channel, it becomes the primary mechanism for momentum exchange, as both shear stress and secondary currents intensity decrease, reduces the mixing layer width and limits its longitudinal growth (Proust et al., 2013, 2017; Proust & Nikora, 2020), and induces flow tridimensionality (Mera et al., 2015). Altogether, the presence of mean transverse flow affects the lateral exchanges of mass and momentum.

Solute transport is influenced by relative flow depth, vegetation (Farzadkhoo et al., 2019; Hamidifar et al., 2015; Nepf, 1999), and mean transverse flow (Shiono et al., 2003). Under non-vegetated conditions, solute transversal spread is greater in the main channel than in the floodplain Shiono et al. (2003). With vegetation present in the floodplain, flow velocity is reduced, which enhances pollutant dilution in the floodplain and affects longitudinal dispersion in the main channel as the flow accelerates in this region (Farzadkhoo et al., 2019; Hamidifar et al., 2015). Changes in vegetation characteristics, such as density, also affect solute spread. In emergent vegetation, sparse densities favor turbulent transport (aka. turbulent diffusion), whereas under dense conditions the contribution of mechanical dispersion becomes significant (Nepf, 1999). Additional factors, including the spatial distribution of vegetation and variations in discharge, may further influence solute tracer transport.

Natural forests exhibit horizontal and vertical distribution heterogeneity, with different species forming a mosaic of plants (Burrows, 1991). This heterogeneity in the horizontal distribution causes local flow effects in the floodplain region, as flow accelerates or decelerates due to the vegetation. Traditional analytical models for depth-averaged streamwise velocity profiles assume uniform vegetation arrays or non-vegetated conditions (Fernandes et al., 2014; Hu & Zhang, 2022; Shiono & Knight, 1991), in which, often a high data resolution is required in zones of high gradients. This imposes limitations as uniform plant distribution is uncommon in natural forests and the acquisition of high data densities can be costly at larger scales. Therefore, a model is needed to describe the transverse profile with sparse data and heterogenous vegetation distributions, which allows the representation of conditions closer to the ones found in nature. The model should, also, account for flow

10.1029/2024WR038968

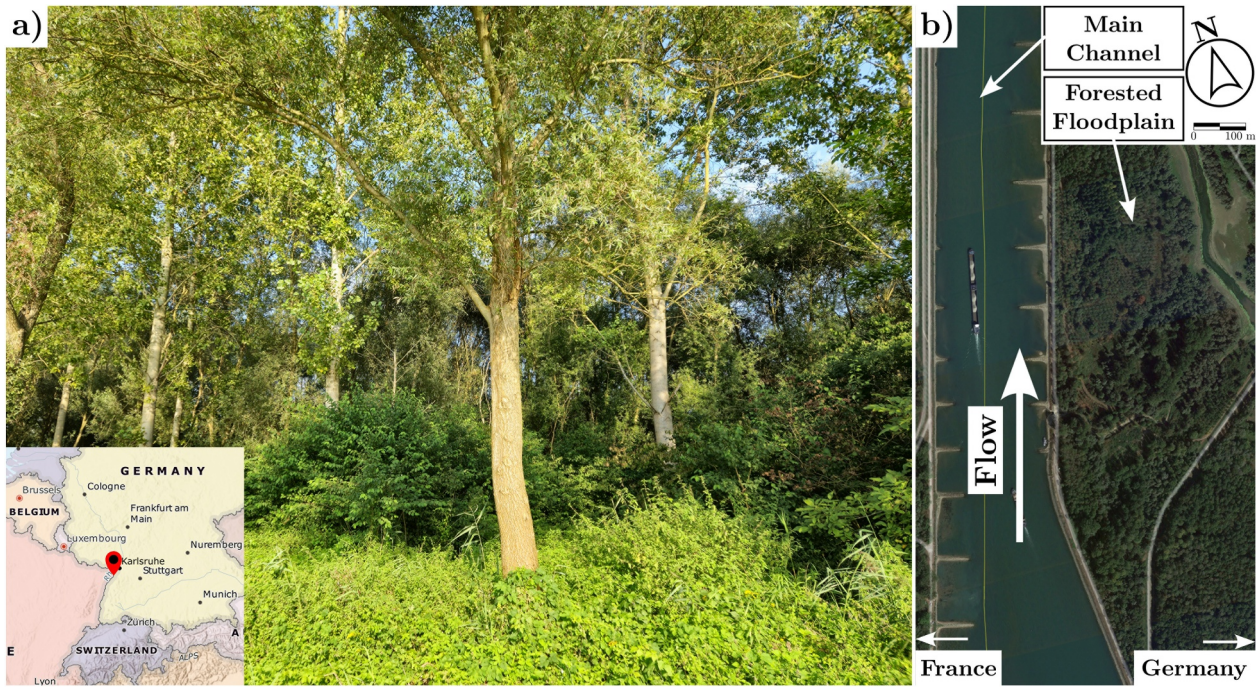

Figure 2. (a) Field photo of the surveyed area [Rastatt, Germany (48°51′09.0″N 8°07′11.0″E WGS 84)] and (b) satellite photo (extracted from Google Earth, image from 17 September 2018).

asymmetry in the mixing layer formed between floodplain and main channel (Dupuis et al., 2017a, 2017b; Proust & Nikora, 2020; Truong & Uijttewaal, 2019; van Prooijen et al., 2005).

Despite its importance, the effects of forest succession on the hydrodynamics of compound channels have not been studied. Furthermore, existing studies on vegetated compound channels often rely on idealized conditions that do not accurately represent natural forests. As a result, forest density and spatial distribution heterogeneity may be misrepresented, potentially skewing the assessment of floodplain forest's impact on compound channel flow. Additionally, these idealized conditions fail to evaluate the effects of forest management practices or provide alternatives for describing the mean flow under the influence of localized vegetation effects.

In this study, we experimentally investigate the hydrodynamics of a natural floodplain forest, focusing on the impacts of its successional development at four distinct life stages, as well as forest management effects. The forest composition and flood depth under investigation were based on a natural floodplain forest in the Upper Rhine. Our analysis considers variables describing both vegetation coverage and hydrodynamics, including forest age, forest management, and relative water depth. We aim to relate these characteristics to their impacts on flow structure, flood risk, navigability, and hydraulic modeling. Furthermore, we highlight the implications for turbulence, the mixing layer as well as mass and momentum exchanges. Additionally, we developed a model to describe the mean streamwise velocity profile under conditions of heterogeneous vegetation positioning. Finally, the effects of vegetation-induced flow readjustments on hydrodynamics and mixing are summarized in a conceptual model that highlights the distinct flow zones introduced by the forest.

2. Field Survey and Vegetation Scaling

2.1. Field Survey

The present experimental research floodplain forest composition and floodplain flow depth are based on a segment of the Upper Rhine River. The reference river reach lies within the floodplain downstream of the Iffezheim dam (Rhine km 334, coordinates 48°51′09.0″N 8°07′11.0″E, WGS 84) in Rastatt, Germany, the most downstream large barrage in the river Rhine (Figure 2). This area is a part of the "Rastatter Rheinaue" natural reserve. The studied reach exhibits high discharge levels during the early summer months, primarily attributable to the seasonal snowmelt occurring in the Alps (Dister et al., 1990). This river reach, and overall the Rhine, has

Table 1
Surveyed Characteristics of the Floodplain Forest

Tree age	N_t [−]	D_t [m]	H_t [m]	$D_{t,m}$ [m]	$H_{t,m}$ [m]	P_i [%]
Adult	467	0.26–0.55	12.7–17.3	0.364	14.82	87.3
Young	68	0.016–0.045	3.0–5.3	0.029	1.85	12.7

Note. N_t is the number of individuals, $P_i = N_t/(N_a + N_y)$ is the adult/young trees proportion, N_a is the number of adult trees, N_y is the number of young trees. The subscript m represents the weighted averaged values of both quantities, among all sub areas.

suffered substantial alteration throughout the 19th and 20th centuries, characterized by extensive rectification efforts and the construction of dikes and barrages (Ochs et al., 2020), and thus, distinct geomorphological types developed. The segment is situated in the pre-channelized transition area between the braided zone (Basel-Rastatt) and the meandering zone (Diaz-Redondo et al., 2017; Dister et al., 1990). In the closest measuring station (Hauenstein, Germany), the average flow discharge was 950 m^3/s, from 1924 to 2024 (LUBW, 2024). Additionally, the minimum observed flow discharge was 404 m^3/s and the maximum 3,451 m^3/s. In the surveyed area, the observed averaged flood level was 2.60 m in the floodplain, which corresponds to a flood event with a return period between 15 and 20 years.

The forest survey, conducted by Hutter (2018), covered an area of 1 ha, demarcated into 16 plots measuring 25 m × 25 m each (Figure 2). Within this area, a total of 535 trees were recorded, and their stems measured in trunk diameter at breast height (D_t), tree height (H_t), and basal area (B). Upon aggregation of data from individual plots, mean values were computed for the total surveyed area, and trees were categorized into two distinct groups: adult trees, characterized by $D_t > 0.10$ m, and young trees, with D_t ranging from 0.01 to 0.10 m (Table S1 in Supporting Information S1). A synopsis of the weighted mean characteristics for both tree groups is presented in Table 1. The surveyed forest ecosystem predominantly comprises *Salix alba* (90% of the population), *Populus canadensis*, *Crataegus laevigata*, *Prunus spinosa*, *Ulmus laevis*, and *Viburnum lantana*. The observed characteristics align with those expected in an area undergoing a secondary succession process, indicative of a forest ecosystem in the mid age, observed by the dominance of *Salix alba* in the tree layer (Dister, 1980; Ochs et al., 2020).

2.2. Vegetation Scaling

In the laboratory scale flume, adult trees were represented by employing rigid PVC cylinders with a diameter $D_r = 2$ cm and a smooth surface, while young trees were represented by flexible silicone elements. The flexible vegetative elements had a height of 6 cm and featured 16 flexible flags, each measuring 4.4 cm in length, 1 cm in width, and 0.1 cm in thickness, arranged along four axes. An additional 2 cm of height constituted the base of the element, facilitating its secure fixation onto a grid positioned at the channel bottom. Furthermore, the elements were made of two-component silicone rubber with a Shore hardness of 40 ShA and a density of 1.1 g/cm^3. For comprehensive description of the development and characteristics of the flexible elements cf. Folke (2023) and Folke and Aberle (2024).

The hydrodynamic density (mD, Equation 1) was used to scale the adult trees (Straatsma, 2008). With an average diameter $D_{t,m} = 0.364$ m, the hydrodynamic density of adult trees in the study area is 0.017 1/m. In laboratory conditions, at a scale of 1:30, the hydrodynamic density was $mD_{\text{scaled}} = 0.51$ 1/m, which was then utilized to determine the requisite number of adult trees. Employing Equation 1 with the known parameters D_r, the resultant rigid vegetation density was of 26 cylinders per square meter in the laboratory scale. Conversely, the quantity of flexible elements was directly scaled maintaining the similar proportions of adult and young trees found in the field, as the resistance force exerted by silicone elements ($F = 0.265 \cdot u_m^{1.03}$) solely relies on the scaled velocity, u_m, as delineated by Folke (2023) and Folke and Aberle (2024). The scaled density of flexible elements was 6 trees per square meter. The scaled forest was classified as the Mid age forest. Both the field forest and the laboratory vegetation exhibited similar proportions of vegetation elements, as detailed in Table 1. Figure 3 shows the vegetation patch at the laboratory scale.

$$mD = n \cdot \frac{D_t}{A} \tag{1}$$

where, n [−] is the number of elements per square meter, A [m^2] is the surveyed area.

3. Experimental Setup and Instrumentation

3.1. Channel and Flow Conditions Description and Mixing Layer Identification

The experiments were conducted at the Federal Waterways Engineering and Research Institute (BAW, Karlsruhe, Germany), in a 30 m long and 5 m wide asymmetric compound channel (i.e., the floodplain is present only at one

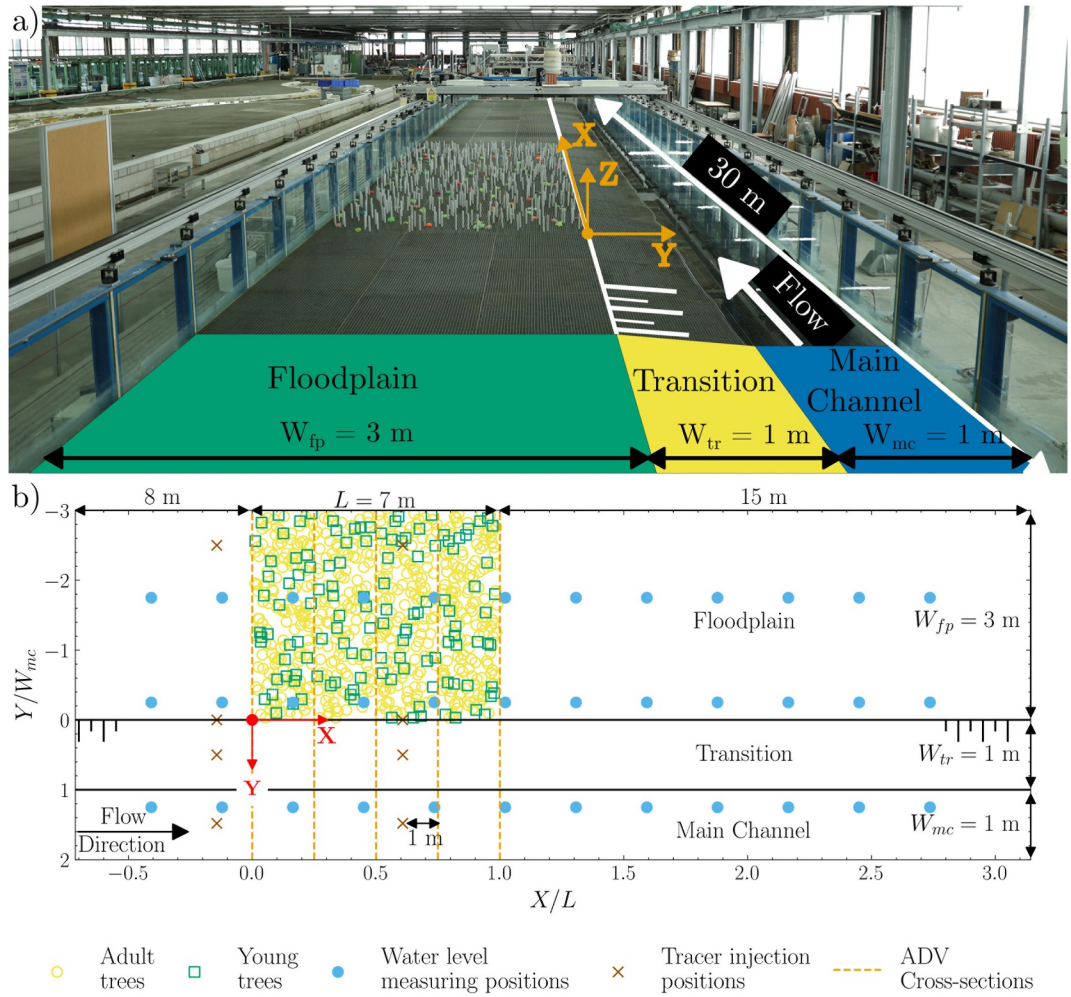

Figure 3. (a) Upstream view of the experimental open channel at BAW and (b) channel top-view sketch with vegetation positioning, planar coordinate system, water level and ADV measuring positions. The occupation of the floodplain in (a, b) corresponds to the Mid age forest.

side of the channel) with a longitudinal bed slope of 0.05% (Figure 3). The cross-sectional layout of the channel comprises three distinct zones, including the floodplain ($W_{fp} = 3$ m), an inclined transition (with a lateral slope of 1:10, characterized by $W_{tr} = 1$ m width and $H_{tr} = 0.1$ m height), and the main channel ($W_{mc} = 1$ m), as depicted in Figures 3 and 4. The channel bottom was constructed in a smooth concrete surface, covered with galvanized steel grids placed on top. Each grid, measuring 1 m x 1 m x 0.25 m, featured 45 subdivisions along the horizontal axis, with holes measuring 0.02 m × 0.02 m, in which the vegetation elements were secured. Both the main channel and floodplain side walls were made of glass.

Discharge was measured at the inlet position utilizing an electromagnetic flow meter (Endress + Hauser—Proline Promag 53 W, with 0.2% of uncertainty). The water level was controlled by two downstream adjustable flap weirs at the end of the channel. No difference between weir one and weir two was set. Experimental trials were conducted under conditions of uniform flow, ensuring consistency and reproducibility of results. To mitigate flow irregularities at the inlet section, a combination of pipes and a honeycomb grid was employed to homogenize the incoming flow.

The flow was kept under subcritical and turbulent conditions in the entire channel. Two flow discharges were investigated Q_1 = 173.2 l/s, based on the average floodplain water depth in the reference reach in the past 20 years, and $Q_2 = 249.3$ l/s. These correspond to bulk flow velocities of $U = 0.24$ m/s for intermediate flow and $U = 0.32$ m/s for deep flow conditions, respectively. The flow was classified according to its relative depth ratio:

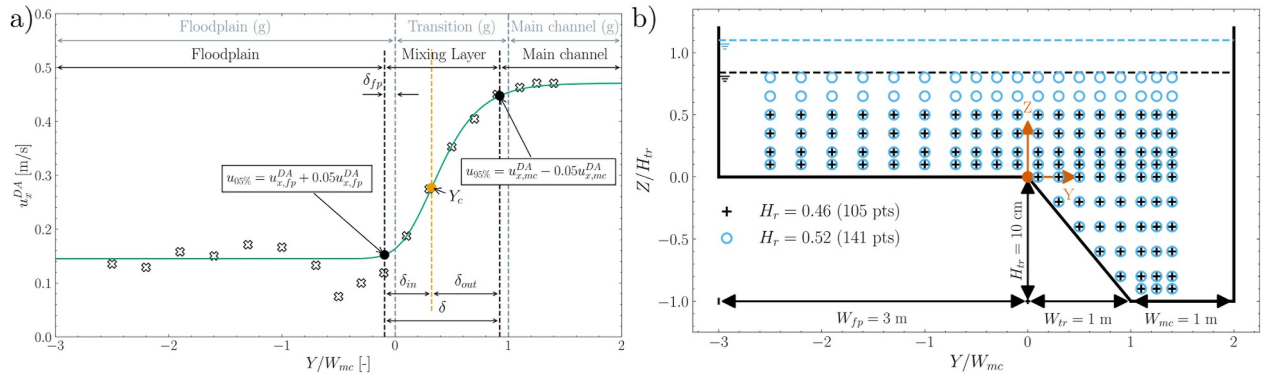

Figure 4. (a) Sketch of the mixing layer and channel division, the g stands for geometrical division, and (b) channel cross-section and ADV velocity measuring grid. The ADV measuring grid is different for the two flow cases.

$H_r = 0.46$ and 0.52 for Q_1 and Q_2, corresponding respectively to intermediate and deep flow conditions (Nezu et al., 1999). The Reynolds number ($Re_i = u_i H_i/\nu$, where i = fp or mc, and ν is the kinematic viscosity) and Froude number ($Fr_i = u_i/\sqrt{gH_i}$, where g is the gravitational acceleration) were calculated for the floodplain and main channel and, together with the values of flow depth, mean velocities and flow rate, are listed in Table 2. The cross-sectional channel division was made based on the mixing layer (ML, Figure 4a), which is a region of high velocity gradient between the floodplain and main channel. In our study, the floodplain and main channel regions are defined outside the mixing layer, as the lateral gradient of the streamwise velocity is lower (Figure 6). The mixing layer was identified with the adjustment of the Unified-Richards function (Tjørve & Tjørve, 2010, 2017) to the lateral profile of the depth-averaged streamwise velocity:

$$u_x^{\mathrm{DA}}(y) = \Delta u \cdot \left(1 + (d-1)\cdot \exp\left(\frac{-k\cdot(y - Y_c)}{\Delta u \cdot \gamma}\right)\right)^{1/(1-d)} + u_{\mathrm{fp}}$$
$$\gamma = d^{d/(d-1)} \tag{2}$$

where, $\Delta u = u^{\mathrm{DA}}_{x,\mathrm{mc}} - u^{\mathrm{DA}}_{x,\mathrm{fp}}$ [m/s] is the depth-averaged velocity difference between the main channel and floodplain ($u^{\mathrm{DA}}_{x,\mathrm{mc}}$ is the maximum depth averaged streamwise velocity in the main channel and $u^{\mathrm{DA}}_{x,\mathrm{fp}}$ is the mean depth averaged streamwise velocity in the floodplain), k [1/s] is the maximum value of the transversal depth-averaged velocity gradient ($\partial u^{\mathrm{DA}}_x/\partial y_{\max}$), Y_c [m] is the coordinate where k value occurs, which coincides with the inflection point, $d > 0$ [−] is the parameter that controls the asymmetry. All curve parameters were adjusted with a weighted least squares method, in which the weights ($W = 1/u^{\mathrm{DA}}_x$) account for a non-uniform variance.

The mixing layer was then determined as the region where the velocities are 5% higher than the sub-section averaged streamwise velocity in the floodplain ($u_{5\%} = u^{\mathrm{DA}}_{x,\mathrm{fp}} + 0.05u^{\mathrm{DA}}_{x,\mathrm{fp}}$) and 5% below the maximum velocity in the main channel ($u_{95\%} = u^{\mathrm{DA}}_{x,\mathrm{mc}} - 0.05u^{\mathrm{DA}}_{x,\mathrm{mc}}$) (Truong & Uijttewaal, 2019; van Prooijen et al., 2005). The threshold of 5% was chosen to account for regression errors, which are in the same order of magnitude as the mass

Table 2
Flow Conditions

Flow	Q [l/s]	H_{fp} [mm]	H_r [−]	U [m/s]	$u^{\mathrm{DA}}_{x,\mathrm{mc}}$ [m/s]	$u^{\mathrm{DA}}_{x,\mathrm{fp}}$ [m/s]	Fr [−]	Fr_{mc} [−]	Fr_{fp} [−]	Re [−]	Re_{mc} [−]	Re_{fp} [−]
Intermediate	173	84	0.46	0.24	0.38	0.20	0.22	0.28	0.22	26,548	69,707	17,375
Deep	249	110	0.52	0.32	0.43	0.28	0.25	0.30	0.27	41,859	90,972	31,185

Note. The subscripts $i = \{-, \mathrm{fp}, \mathrm{mc}\}$ refer to the whole cross-section, floodplain and main channel, respectively.

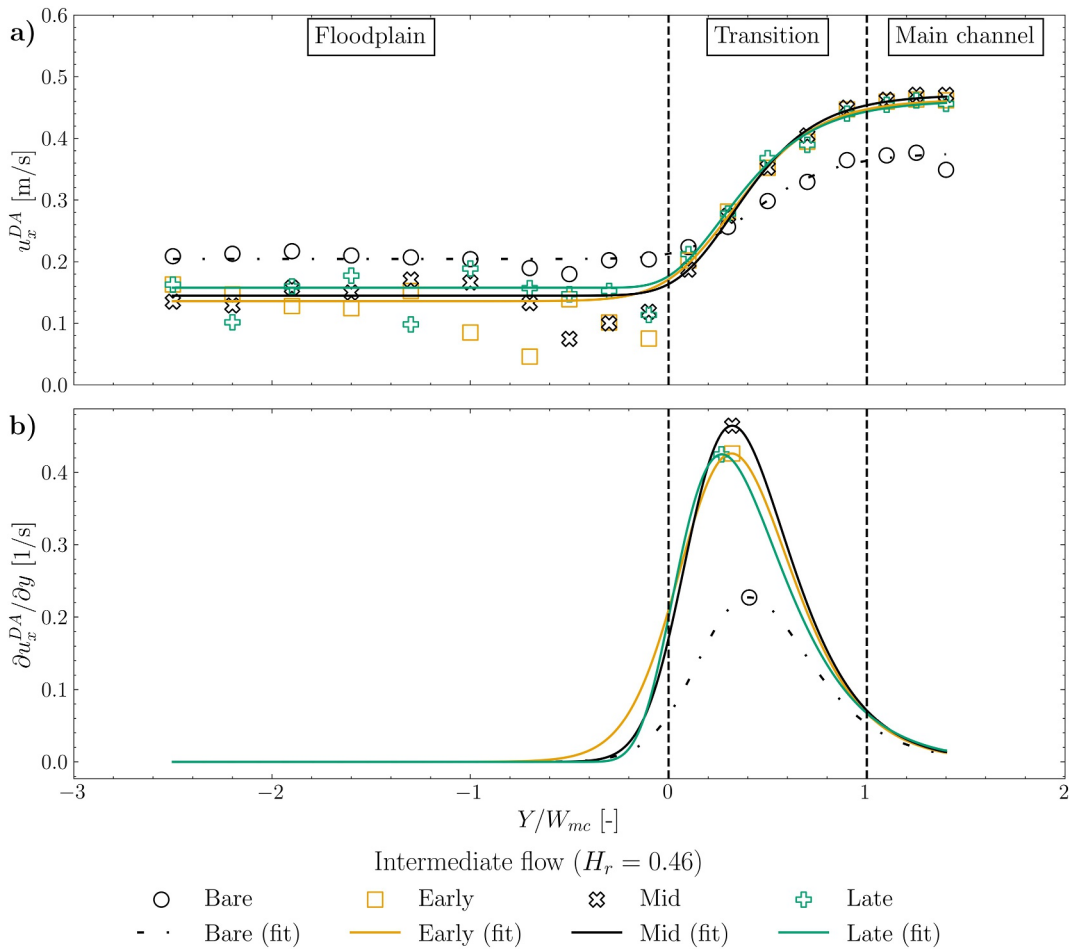

Figure 5. Transversal depth-averaged velocity profile fitted with the Unified-Richards function at $X/L = 1.00$, for all forest ages in the intermediate flow ($H_r = 0.46$) (a) Fitted curve and measured streamwise velocity (u_x^{DA}) profile and (b) transversal velocity gradient ($\partial u_x^{\mathrm{DA}}/\partial y_{\max}$) with indication of its maximum value.

conservation difference between the cross-sections. The mixing layer center position is defined as the inflection point, which coincides with Y_c. The depth-averaged velocity at mixing layer center (u_c^{DA}) can be determined as:

$$u_c^{\mathrm{DA}} = \Delta u \cdot d^{1/(1-d)} + u_{x,\mathrm{fp}}^{\mathrm{DA}} \tag{3}$$

3.2. Water Level and Velocity Measurements

Water level was measured using ultrasonic sensors, with a standard measurement error of approximately 0.1 mm and an interrogation wave of 220 kHz. The measurement positions were spaced 2 m apart in the streamwise direction. In the transverse direction, three positions were measured, $Y/W_{\mathrm{mc}} = -1.75$, -0.25 and 1.25 (blue circles, Figure 3b). Each depth series was measured for 20 min at a rate of 1 Hz, and a total of five series were measured for each forest age and three series for the Bare scenarios.

Velocity measurements have been conducted using single-point ADV using an automated transversing system. The three-dimensional ADV, Nortek Vectrino+, had a side-looking configuration, with a sampling volume located 5 cm away from the probe. To determine the time required for statistical convergence, 600 s of data were acquired, and a cumulative time-averaging procedure was used to verify the minimum required duration of 150 s. Each measuring point was recorded at 200 Hz for 180 s (36,000 samples) and three instantaneous velocity components were captured (u_x, u_y and u_z). The flow was seeded with polyamide particles (KVS Vestosint) with a median diameter of 40 μm to increase the ADV signal correlation (>70%) and signal-to-noise ratio

Table 3
Vegetation and Flow Characteristics of the Test Scenarios

Case	H_{fp} [mm]	H_r [−]	Flow	Age	n_y [−]	n_a [−]	P_y [%]	mD [m^{-1}]	LAI [−]	Φ [%]
1	84	0.46	Intermediate	Bare	–	–	–	–	–	–
2	84	0.46	Intermediate	Early	18	8	69.2	0.16	0.6	0.4
3	84	0.46	Intermediate	Mid	6	26	18.8	0.52	0.2	0.9
4	84	0.46	Intermediate	Late	2	10*	16.7	0.45	0.1	1.6
5	84	0.46	Intermediate	Mid-Only-Young	6	–	100	–	0.2	0.1
6	84	0.46	Intermediate	Mid-Only-Adult	–	26	–	0.52	–	0.8
7	110	0.52	Deep	Bare-High	–	–	–	–	–	–
8	110	0.52	Deep	Mid-High	6	26	18.8	0.52	0.2	1.1

Note. *Adult vegetation diameter is increased from $D_t = 2$ cm to $D_t = 4.5$ cm.

(SNR > 15 dB). Data quality and time-averaging procedures were assessed using the VIPER code (Sokoray-Varga, 2022), which applies the phase-space thresholding despiking technique (Goring & Nikora, 2002). After point quality control, if more than 30% of a measured velocity time series was removed, the point was remeasured until all quality criteria were satisfied. The ADV measurements were carried out at two spatial densities of 166 points/m^2 and 202 points/m^2, for the intermediate and deep flows respectively (Figure 4). At each cross-section, measurement points were spaced at intervals of 0.30 m on parts of the floodplain ($Y/W_{mc} < -0.70$) and 0.20 m in other regions. In the vertical direction on the floodplain, four measurement points were taken for intermediate flow conditions, with an additional two points captured for deep flow conditions. Along the longitudinal axis, velocity measurements were obtained at five cross-sections with uniform spacing of 1.75 m for the vegetated conditions and at two cross-sections ($X/L = 0$ and 1) for Bare conditions (Figure 3).

The transverse velocities (u_y and u_z) had a relatively smaller magnitude compared to the streamwise velocity (u_x). Hence, the misalignment of the ADV probe can introduce significant errors, on the order of $O(10^3)$, in those components (Peltier, Rivière, et al., 2013). The angle correction was performed with the channel under non-vegetated conditions for both flow conditions (Cases 1 and 7, cf. Table 3). During the angle correction, it was assumed that the spatial-averaged velocity u_y was zero at the geometrical main channel ($Y/W_{mc} > 0$), while the vertical component u_z approached zero near the channel bottom, following the approach from Proust and Nikora (2020). This procedure resulted in the correction angles of $\alpha_{rot,1} = -3.42°$ vertical-axed, $\beta_{rot,1} = -1.13°$ (spanwise-axed) and $\gamma_{rot,1} = -1.65°$ (streamwise-axed) in the first measurements (before October/2023) and $\alpha_{rot,2} = 0.06°$, $\beta_{rot,2} = -1.36°$ and $\gamma_{rot,2} = 0.40°$, in the second measurements (after December/2023).

3.3. Floodplain Vegetation Design

In this study, four moments in the life of a forested floodplain were investigated: Bare (not vegetated), Early, Mid, and Late ages. Furthermore, we investigated the influence of the relative depth (*Bare-High* and *Mid-High*) and the isolated effect of flexible and rigid vegetation on the Mid age forest (*Mid-Only-Young* and *Mid-Only-Adult*) (Table 3).

The forest spanned along the entire floodplain width and, in the streamwise direction, it had a length of $L = 7$ m (Figure 3). The forest composition at various stages of development was designed on a scaled-down representation of the natural forest described in § 2.2, hereinafter called Mid age forest. The Early and Late succession stage scenarios were derived from the Mid age forest, based on the values of mD, the leaf area index (LAI, Equation 4) and the proportion between adult and young trees ($P_y = n_y/(n_a + n_y)$). At the Early age, the forest was mainly composed of young trees and few adult individuals, while at the Late age the forest had adult trees with an increased diameter (attachment of 4 rigid elements, comprising a diameter $D_r = 4.4$ cm) which were predominant over the young trees. The stem diameter is inversely proportional to the hydrodynamic density (Folke, 2023). This criterion was adopted to determine the number of adult trees in the Late age, where mD values were lower than in the Mid age. For the Late age, the forest density decreases (in terms of LAI) as the adult trees suppresses the growth of new plants, however the bigger diameter conserves the values of mD and increase the solid volume fraction (ϕ, Equation 5), as shown in Table 3.

Table 4
Summary of the Sub Section-Averaged Flow Characteristics at X/L = 1.00

Case	H_r [−]	Age	$u_{x,\mathrm{mc}}^{\mathrm{DA}}$ [m/s]	$u_{x,\mathrm{fp}}^{\mathrm{DA}}$ [m/s]	λ [−]	k [1/s]	Fr_{mc} [−]	Fr_{fp} [−]	Re_{mc} [−]	Re_{fp} [−]
1	0.46	Bare	0.38	0.20	0.30	0.23	0.28	0.22	69,707	17,375
2	0.46	Early	0.46	0.14	0.55	0.43	0.34	0.15	85,739	11,543
3	0.46	Mid	0.47	0.14	0.53	0.46	0.35	0.16	87,029	12,253
4	0.46	Late	0.46	0.16	0.49	0.43	0.34	0.17	85,445	13,375
5	0.46	Mid-Only-Young	0.41	0.19	0.35	0.27	0.30	0.21	75,004	16,558
6	0.46	Mid-Only-Adult	0.46	0.15	0.50	0.44	0.34	0.17	84,226	13,026
7	0.52	Bare-High	0.43	0.28	0.21	0.22	0.30	0.27	90,972	31,185
8	0.52	Mid-High	0.56	0.20	0.48	0.57	0.39	0.19	118,339	21,587

$$\mathrm{LAI} = A_L / A_B \tag{4}$$

$$\phi = \frac{n_a \cdot V_a + n_y \cdot V_y}{L \cdot W_{\mathrm{fp}} \cdot H_{\mathrm{fp}}} \tag{5}$$

where, A_L [m^2] is the one-sided leaf area and A_B [m^2] is the ground area, V_i [m^3] is the single element volume.

The vegetation positioning was randomized independently in blocks of 1 m^2, with a few constraints for both practical and biological competition considerations. The constraints ensured a minimum distance of D_r between adjacent tree elements and avoided the placement of elements along the borders of the grid for practical considerations. Figure 3 illustrates the arrangement of vegetation at the Mid age, while the placements for all other forest ages are presented in Figure S1 of Supporting Information S1 (c.f. Supporting Information S1).

Four floodplain forest ages were investigated, to represent the development from Bare (non-vegetated, reference case) to a Late forest age (Figure 1), investigated in cases 1 through 4. Moreover, the isolated impact of each tree type on the Mid age was explored in cases 5 and 6, in which based on the Mid age there was a removal of all adult or young trees. Finally, the impact of flood depth was investigated comparing cases 1, 3, 7 and 8. The specifics of the corresponding investigated flood depths, vegetation compositions, adult hydrodynamic density (mD), young leaf area index (LAI) and solid volume fractions are listed in Table 3.

4. Results

The flow description and main hydrodynamic results are presented in this section, with corresponding plots provided in Supporting Information S1.

4.1. Streamwise Velocity

For the Bare and *Bare-High* scenarios, the depth-averaged streamwise velocity (u_x^{DA}), for the different forest ages at $X/L = 1.00$ had a monotonic velocity profile (Figure S2 in Supporting Information S1). This finding aligns with Juez et al. (2019) and Proust et al. (2017), both of whom studied asymmetrical channel configurations. However, the non-monotonic behavior of intermediate flows observed by Stocchino and Brocchini (2010) and Nezu et al. (1999) was not observed in our data, most attributable to transversal inclination angle in the transition region, that in their cases were 90°. Due to the randomized vegetation positioning, local velocity effects are visible, characterized by flow deceleration in the presence of vegetation and flow acceleration in its absence, as observed in the Mid and *Mid-High* cases. The forest reduced the flow velocities in the floodplain and increased them in the main channel, due to the increased hydraulic roughness in the floodplain. Compared to the Bare conditions, the forest effect was more pronounced under the deep flow for the main channel regions (Table 4).

The forest induced a stronger shear at the interface zone, as observed in the velocity slope at the transition region. The increase in lateral velocity across all ages was confirmed by the maximum values of the transversal velocity gradient ($\partial u_x^{\mathrm{DA}} / \partial y_{\max}$) and the dimensionless shear, also known as the velocity ratio λ (cf. Table 4). These findings are consistent with Truong and Uijttewaal (2019) and Truong et al. (2019), and this phenomenon is associated with

the increased drag in the floodplain region. Furthermore, the shear was inversely proportional to H_r, confirming the findings by Proust et al. (2017). Table 4 summarizes the averaged velocities at the floodplain and main channel, the dimensionless shear (λ), and the maximum transversal velocity gradient ($k = \partial u_x^{\mathrm{DA}}/\partial y_{\max}$).

The lateral profile of the depth-averaged streamwise velocity was fitted to a Unified-Richards function (Equation 2). This function was chosen for three main reasons: (a) it allows for the calculation of an averaged velocity in both the floodplain and main channel regions, minimizing the local effects produced by non-uniform vegetation placement, (b) it can describe the profile asymmetry at the mixing layer region and (c) it requires few parameters to fit. Regarding (a), the averaged profile that the model provides is in accordance with lateral profiles with and without vegetation (Juez et al., 2019; Truong et al., 2019; Truong & Uijttewaal, 2019). Regarding point (b), traditional fittings of shear flow lateral velocity profiles using the hyperbolic tangent, as applied in lateral cavities (Sukhodolov et al., 2017) or sheared flows (Sukhodolov et al., 2010), cannot be directly implemented for compound channels, as the internal part of the mixing layer is typically smaller than the outer part (Dupuis et al., 2017a, 2017b; Proust & Nikora, 2020; Truong & Uijttewaal, 2019; van Prooijen et al., 2005). Compound channel models based on the momentum equation, such as the SKM (Shiono & Knight, 1991) and the improved Lateral Distribution Method (LDM) (Fernandes et al., 2014), were fitted to our data. For the Bare and Bare-High scenarios, both the LDM and SKM models had an RMSE/$U \cong 8\%$. For all vegetated conditions, both models could not be fit to the experimental data. This lack of fitting was attributed to the lateral distance between the vertical profiles, the high gradients introduced by the vegetation local effects due to the natural vegetation distribution, and the presence of a mean transverse flow. Regarding point (c), the Unified-Richards function requires only the velocity and the total width of the channel, using physical parameters to fit the data. This approach is advantageous in conditions of data scarcity and with the presence of mean transverse flow, as it allows for the direct interpretation of crucial flow information, such as the maximum transversal gradient of the streamwise velocity ($\partial u_x^{\mathrm{DA}}/\partial y_{\max}$).

Figure 5 shows the Unified-Richards function applied to the four moments of the forest with intermediate flow. In addition to enabling the fitting of sparser and heterogeneous data, our model allowed for the direct calculation of the maximum lateral velocity gradient and the inflection position, parameters that can be used to determine mixing layer (ML, Figure 4a) properties and to divide the channel between the floodplain and main channel. The model's asymmetric sigmoid shape facilitated the description of the homogeneous flow profile in the main channel and transition region while simultaneously capturing bulk information from the heterogeneous flow in the floodplain. The model effectively described the mean flow behavior across all measured cross-sections. In terms of mass conservation, we observed differences ranging from -4.1% to $+1.8\%$, when comparing the most upstream with the most downstream cross-sections of each scenario. Overall, the model provided a good fit to the data, with a $R^2 = 0.85$–0.99 and RMSE/$U = 2.5\%$–14.4%. Finally, the model provided adequate flow description for situations with and without vegetation presence.

Based on the Unified-Richards approach, the sub-section averaged streamwise velocities ($\tilde{u}_x$) were calculated, with each sub-section defined in regions outside the mixing layer. This division isolates the effect of each sub-section, thereby minimizing the influence of regions with high lateral gradients in the streamwise velocity (Figure 5). Under Bare conditions, the velocity remained relatively constant across both cross-sections in the absence of mean transverse flow (Figure S4 in Supporting Information S1), indicating that the flow is fully readjusted. In contrast, the presence of forest vegetation introduced a longitudinal evolution of the flow in both regions, primarily due to adjustments triggered by changes in roughness (Dupuis et al., 2017a; Rominger & Nepf, 2011). In the floodplain, the most pronounced evolution occurred during the Early age, followed by the Mid and Late ages (Figure S3 in Supporting Information S1), in accordance with the dimensionless shear (Table 4). In the forest management cases, the *Mid-Only-Young* scenario exhibited smaller change in both sub-sections when compared to the *Mid-Only-Adult* case. This was attributed to the lower flow blockage observed in the *Mid-Only-Young* scenario (Table 3). Additionally, an increase in the relative water depth H_r led to higher velocities in the *Bare-High* and *Mid-High* scenarios, attributable to the reduced hydraulic roughness in the floodplain (cf. Table 5). This decreased roughness is associated with an extension layer above the young trees, where only the adult trees contribute to flow resistance in the *Mid-High* scenario, and with the reduced bottom roughness observed in both cases. In the main channel, the evolution of velocity remained quasi-linear across all forest ages. Under non-vegetated conditions, the value $\tilde{u}_x/U$ was higher in deep flow due to a reduced topographical influence. This

10.1029/2024WR038968

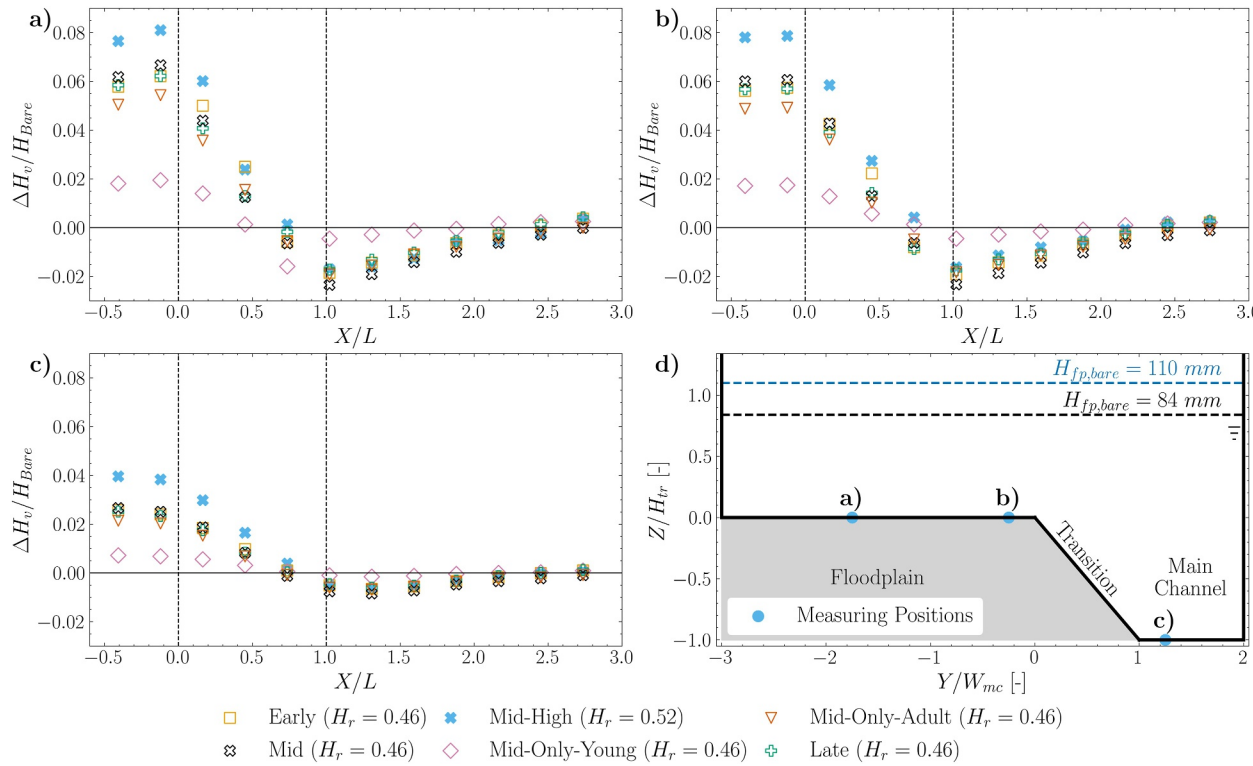

Figure 6. Longitudinal distribution of the depth change ($\Delta H = H_v - H_{bare}$), where H [m] is the depth and the subscripts v and bare stand for vegetated and non-vegetated, respectively. (a) the inner floodplain ($Y/W_{mc} = -1.75$), (b) outer floodplain ($Y/W_{mc} = -0.25$), (c) the main channel ($Y/W_{mc} = 1.25$). Finally, (d) represents the measuring position in the cross-section. The dotted lines (a–c) represent the limits of the vegetation patch of length $L = 7$ m.

reduced influence, combined with faster flow, yielded conditions that are closer to uniformity compared to those observed in intermediate flows. Further details on uniformity are discussed in §5.4.

4.2. Mean Transverse Flow

A mean transverse flow appeared as the flow readjusted to the introduction of vegetation in the floodplains, as a consequence, in both Bare conditions, no mean transverse flow was observed. The introduction of the forest created a current from the floodplain into the main channel, which is associated with the increased downstream hydraulic roughness in the floodplain and the consequent flow adjustment. At the center of the mixing layer Y_c, a consistent maximum in the time- and depth-averaged transverse velocity u_y^{DA} was measured at $X/L = 0.25$ (Figure

Table 5
Main Characteristics of the Mixing Layer: Total (δ), Inner (δ_{in}) and Outer (δ_{out}) Widths, Position of the Center Normalized by the Width of the Main Channel (Y_c/W_{mc}), Penetration Into the Floodplain (δ_{fp}/δ), Determined for the Cross-Section $X/L = 1.00$

Case	H_r [−]	Age	u_c^{DA} [m/s]	δ [m]	δ_{out} [m]	δ_{in} [m]	δ_{in}/δ [%]	Y_c/W_{mc} [−]	δ_{fp}/δ [%]
1	0.46	Bare	0.28	0.88	0.50	0.38	43.2	3.41	0.0
2	0.46	Early	0.28	1.15	0.59	0.56	48.5	3.32	24.0
3	0.46	Mid	0.28	1.02	0.60	0.42	40.9	3.32	9.4
4	0.46	Late	0.27	1.01	0.67	0.34	33.8	3.27	7.2
5	0.46	Mid-Only-Young	0.27	0.99	0.67	0.33	32.9	3.30	3.0
6	0.46	Mid-Only-Adult	0.28	0.98	0.58	0.40	40.4	3.32	7.3
7	0.52	Bare-High	0.34	0.68	0.41	0.27	39.5	3.36	0.0
8	0.52	Mid-High	0.33	0.90	0.60	0.30	33.7	3.26	4.1

S4 in Supporting Information S1). This peak was associated with overall vegetation density and LAI, as young trees produce higher lateral flow blockage. In the sparsest case, *Mid-Only-Young*, the peak was absent, while it was reduced in the Early age case, which had the highest proportion of young trees. At the last cross-section $u_y^{DA} \cong 0$, which is associated with the flow readjustment within the vegetation. The Mid and Late ages had similar magnitudes, being the highest u_y^{DA}, after $X/L > 0$, the Early age decelerated at a lower rate maintaining higher values than the other ages. The conservation of a faster mean transverse flow in the Early age can be associated with the hydraulic roughness, which was higher for this age, especially in the transverse direction as the blockage of young trees was higher than adult ones. As a result, the flow readjusted in a shorter length in the Mid age, as there was a higher number of adult trees. In the *Mid-Only-Young* scenario, the transverse flow remained low compared to the other scenarios, however, u_y^{DA} did not become zero at the end of the forest, as the development region is longer for sparse vegetation with wide patch (Rominger & Nepf, 2011). The increase in relative water depth H_r led to an increase in u_y^{DA} for the vegetated scenario, while in the Bare case it remained zero. In the *Mid-High* case, the increased u_y^{DA} when compared to the Mid scenario, was attributed to the reduced topographical influence and the growth of the flow layer above the young trees.

4.3. Water Depth

Longitudinal profiles of water depth change at three transverse coordinates are plotted in Figure 6. The water depth change is expressed as $\Delta H = H_v - H_{\text{bare,}}$ where H_v is the water depth at each age and H_{bare} is the water depth for the Bare case, which is used as reference case. Since the flow is subcritical throughout the entire domain, the water level is overall controlled by the downstream weirs, being influenced by the roughness of the floodplain. In all forest ages, the depth increased in the region upstream of the forested floodplain in all three transverse Y/W_{mc} coordinates. Inside the forest, the water depth changes decreased longitudinally, until negative values were achieved. Past the forest, the water depth gradually recovered to the observed in the Bare scenarios. This behavior is connected to the downstream roughness, that impacts the water depth changes. Similar findings were observed in Dupuis et al. (2017a); see Figure 3, where, in the flow transition from a low (meadow) to a high (wood) roughness, it also inverted the water depth trend. It is arguable that the depth changes reflect the vegetation effect on the dimensionless shear λ, as even in subcritical conditions, it increases the oscillations in water depth (Proust et al., 2022). Although we concur with the depth changes shown by Proust et al. (2022), our results indicate that the effect of $\partial u_x^{DA}/\partial y_{max}$ seems to be predominant over the λ, when comparing Mid and *Mid-High* cases, in which the maximum λ occurs in the former and the maximum $\partial u_x^{DA}/\partial y_{max}$ in the latter.

The increase in flow rate led to an approximate 2% increase in the maximum flood depth between the intermediate and deep flows, across all transversal regions, followed by a smaller reduction in the flow depth at the end of the forest ($X/L = 1.00$, Figure 6). Moreover, in the deep flow, the downstream vegetation effect was weaker than in the intermediate flow. However, in the intermediate flow, all the ages exhibited a similar magnitude and length required to recover into the H_{bare}. Notably, the depth at the position $Y/W_{\text{mc}} = 1.25$ experienced the smallest change due to the flow acceleration occurring in the main channel region.

4.4. Section-Averaged Turbulent Flow Characterization

In both Bare conditions, the depth-averaged Reynolds stress in the horizontal plane, $-\rho\left(\overline{u_x' u_y'}\right)^{DA}/\left(u_{x,\text{mc}}^{DA} - u_{x,\text{fp}}^{DA}\right)^2$, at $X/L = 1.00$ were close to zero (Figure S5 in Supporting Information S1). In the Bare and *Bare-High* scenarios, a small peak was observed near the center of the mixing layer, with magnitudes lower than those reported for compound channels with a vertical transition (Dupuis et al., 2017a, 2017b). The same peak was not observed in vegetated floodplain conditions. The increase in the relative water depth H_r slightly increased the stress peak in the *Bare-High* case in contradiction with Stocchino and Brocchini (2010). The forest introduced local effects inside the floodplain, associated with the heterogeneous vegetation positioning. The Reynolds stress peak in the transition region commonly found in the literature (Dupuis et al., 2017a, 2017b; Truong et al., 2019; Truong & Uijttewaal, 2019) was absent. This absence was attributed to the presence of a mean transverse flow toward the main channel (Proust et al., 2013, 2017, 2022) and the sloped transition (Xiao et al., 2018), which both reduce the Reynolds stress magnitudes in compound channels.

The turbulence intensities, defined as $TI_x = \left(\overline{u'_x u'_x}\right)^{0.5}/U$ and $TI_y = \left(\overline{u'_y u'_y}\right)^{0.5}/U$, were higher in the main channel at $X/L = 1.00$. Overall, no significant changes were found between the intermediate flow depth scenarios in the main channel, ranging from $TI_{x,mc} = 20.8\%$ to 22.7%, and $TI_{y,mc} = 11.0\%$ to 11.8%. Vegetation reduced the turbulence intensities in the x-direction (TI_x) in the floodplain and increased in the main channel, when compared to Bare conditions. For the y-direction, the main channel values were quasi-constant while in the floodplain it increased for the Early and Late scenarios, while it decreased in the Mid age. In the floodplain, the turbulence intensities ranged from $TI_{x,fp} = 12.1\%$ to 16.6%, and $TI_{y,fp} = 6.5\%$ to 8.6%. The increase in the relative flow depth (H_r) showed negative feedback in the turbulence intensity in all directions, which is associated with a reduction in the dimensionless shear λ (Dupuis et al., 2017a, 2017b; Proust et al., 2022). Similar trends were observed in the normalized turbulent kinetic energy, defined as $TKE/U = (0.5 \cdot tr(\overline{u_i u_j}))^{0.5}$. The pattern of reduction in the floodplain appears to follow the magnitude of the mean transverse flow, which transports momentum toward the main channel (Proust et al., 2017). In summary, our observations indicate that turbulence levels and turbulent kinetic energy in the flow are modulated by three primary factors: (a) mean transverse flow (inversely proportional, and the dominant effect), (b) vegetation characteristics (directly proportional), and (c) relative water depth H_r (inversely proportional).

4.5. Mixing Layer Width

The width of the mixing layer defined in § 3.1 can be analytically calculated with the lateral profile of the depth-averaged streamwise velocity. The mixing layer width was divided into two components: the inner, δ_{in} (Equation 6). and outer, δ_{out} (Equation 7). The total mixing layer width is given by $\delta = \delta_{in} + \delta_{out}$.

$$\delta_{in} = Y_c - \frac{\Delta u \cdot \ln\left(\frac{(d-1)\exp\left[(\gamma \cdot k \cdot Y_c)/\Delta u\right]}{u_{fp}^{(1-d)} \cdot (20\Delta u)^{(d-1)} - 1}\right)}{\gamma \cdot k} \tag{6}$$

$$\delta_{out} = \frac{\Delta u \cdot \ln\left(\frac{(d-1)\exp\left[(\gamma \cdot k \cdot Y_c)/\Delta u\right]}{\left(19u_{mc} - 20u_{fp}\right)^{(1-d)} \cdot (20\Delta u)^{(d-1)} - 1}\right)}{\gamma \cdot k} - Y_c \tag{7}$$

Figure 7 shows the longitudinal evolution of the total mixing layer width δ. The introduction of the forest widened the total mixing layer width (δ) due to the increased dimensionless shear λ (Figure S6 in Supporting Information S1), in agreement with Brown and Roshko (1974). For $X/L < 0.25$, a high growth rate was observed, while for $X/L > 0.25$, the mixing layer width growth rate decreased achieving a quasi-constant width for the rest of the channel in contrast to the Bare conditions that continued to grow. The relative flow depth (H_r) was inversely proportional to the total mixing layer width (δ), due to the reduction in the dimensionless shear λ. This observation is consistent with Dupuis et al. (2023) and Proust et al. (2017, 2022).

Table 5 presents the total, inner and outer mixing layer widths, its center position and velocity, and the penetration into the floodplain at $X/L = 1.00$. In all scenarios, the outer part of the mixing layer was wider than the inner part in all cases (Table 5), in agreement with Dupuis et al. (2017a, 2017b) and Proust and Nikora (2020). The proportion of the inner mixing layer over the total (δ_{in}/δ) was proportional to the dimensionless shear λ, as the Early age had the highest proportion between the successional ages and the *Mid-Only-Adult* in the management scenarios, following the dimensionless shear (λ) trend. The velocity in the mixing layer center u_c^{DA} was not significantly affected by vegetation. The mixing layer center Y_c was displaced toward the floodplain, with shifts ranging from −15 to 6 cm between cross-sections at $X/L = 0.00$ and 1.00. Past an initial displacement toward the floodplain, due to the asymmetrical growth and increase of the dimensionless shear λ, the center slightly shifted toward the main channel in the same direction as the mean transverse flow, in agreement with Dupuis et al. (2017a), and in contrast with Peltier et al. (2013), Proust et al. (2013) and Proust and Nikora (2020), in which the center exclusively moved in the direction of the transverse flow under non-vegetated conditions. Overall, the forest led to an increase in the total mixing layer width δ and a displacement of the mixing layer center toward the floodplain when compared to Bare conditions. Combined, these conditions led to a penetration of the mixing layer in the floodplain (δ_{fp}/δ), not observed in the Bare case (Table 5). The increase in the relative water depth reduced the mixing layer penetration in the floodplain, as the total mixing layer width was narrower than in intermediate flow conditions.

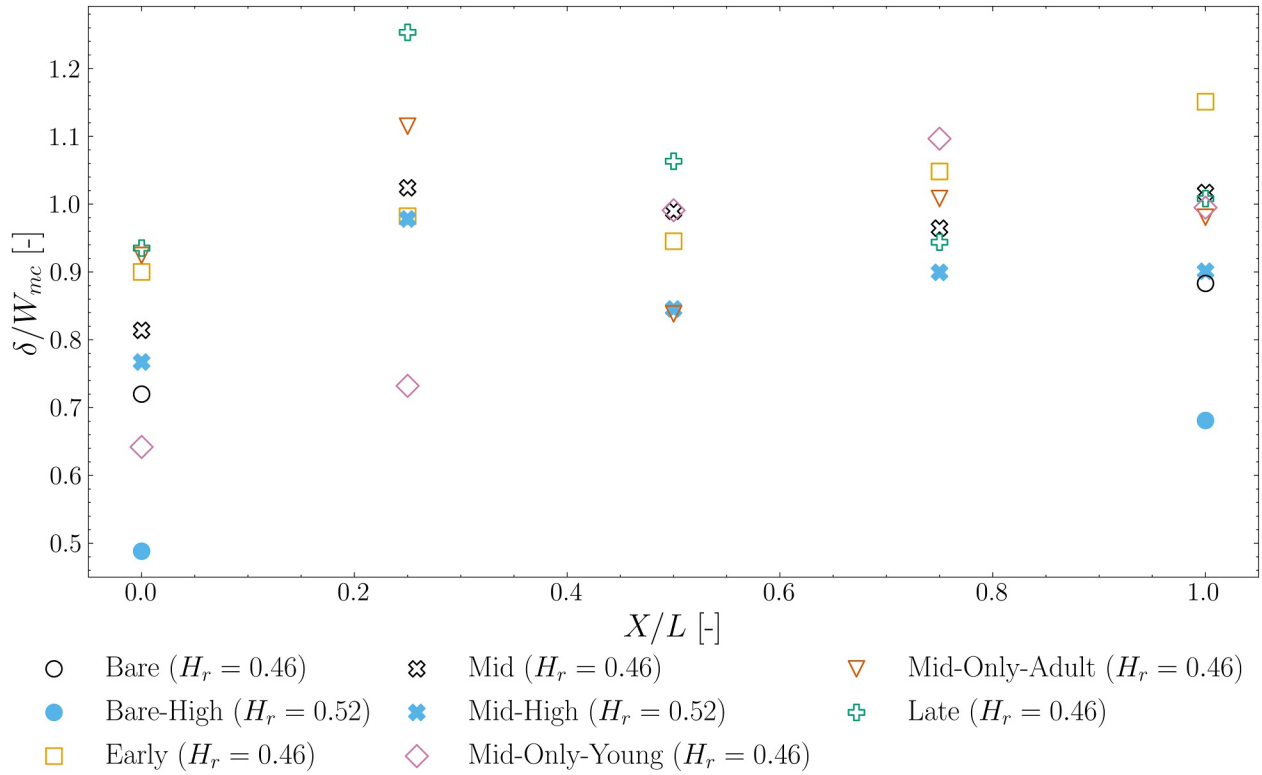

Figure 7. Longitudinal evolution of the normalized total mixing layer width (δ/W_{mc}).

4.6. Transverse Exchange of Mass

The flow discharge (Q) was calculated in each subsection individually, using a geometrical division at $Y/W_{mc} = 0.00$. In each cross-section, the flow discharge was calculated as $Q_i = \ddot{u}_{x,i} \cdot A_{f,i}$, where $\ddot{u}_{x,i}$ [m/s] is the geometrical subsection averaged measured velocity and $A_{f,i}$ [m^2] is the flow area in each subsection, the subscript i refers to the floodplain and main channel. The total flow discharge was calculated as the sum of both subsections, $Q = Q_{mc} + Q_{fp}$. The calculated total flow discharge did not correspond to the channel inlet discharge, as the velocity measuring points did not cover the entire channel cross-section and flow depth (Figure 4). The differences imposed by vegetation in the transverse exchange of mass were investigated by calculating the relative difference in the flow discharge of the vegetated cases compared to Bare conditions, $\Delta Q_{fp} = Q_{fp,v} - Q_{fp,bare}$.

The longitudinal evolution of the floodplain flow discharge change ($\Delta Q_{fp}/Q_{bare}$) compared to the Bare case was negative in all cross-sections, as the flow diverted toward the main channel (Figure 8). The flow diversion promoted an advective mass flux toward the main channel region, as consequence of the flow readjustment to a longitudinal roughness change (Dupuis et al., 2017a; Rominger & Nepf, 2011). The flow imbalance was not linear, as the discharge followed the same tendency as the mean transverse flow u_y^{DA}, which implies a peak in the discharge at $X/L = 0.25$. Past this peak, the flow imbalance had a spatial offset, as the effect of the mean transverse flow u_y^{DA} on the flow discharge was noticeable one cross-section downstream (Figure 8 and Figure S4 in Supporting Information S1), in agreement with Dupuis et al. (2017a), Naghavi et al. (2022) and Peltier, Proust, et al. (2013). Compared to the intermediate flow conditions, the forest effect was more pronounced under the deep flow conditions.

4.7. Transverse Exchange of Streamwise Momentum

The transversal exchange of the total depth-averaged streamwise momentum flux, across the XY-plane (τ_{xy}), is defined as follows (Proust et al., 2013).

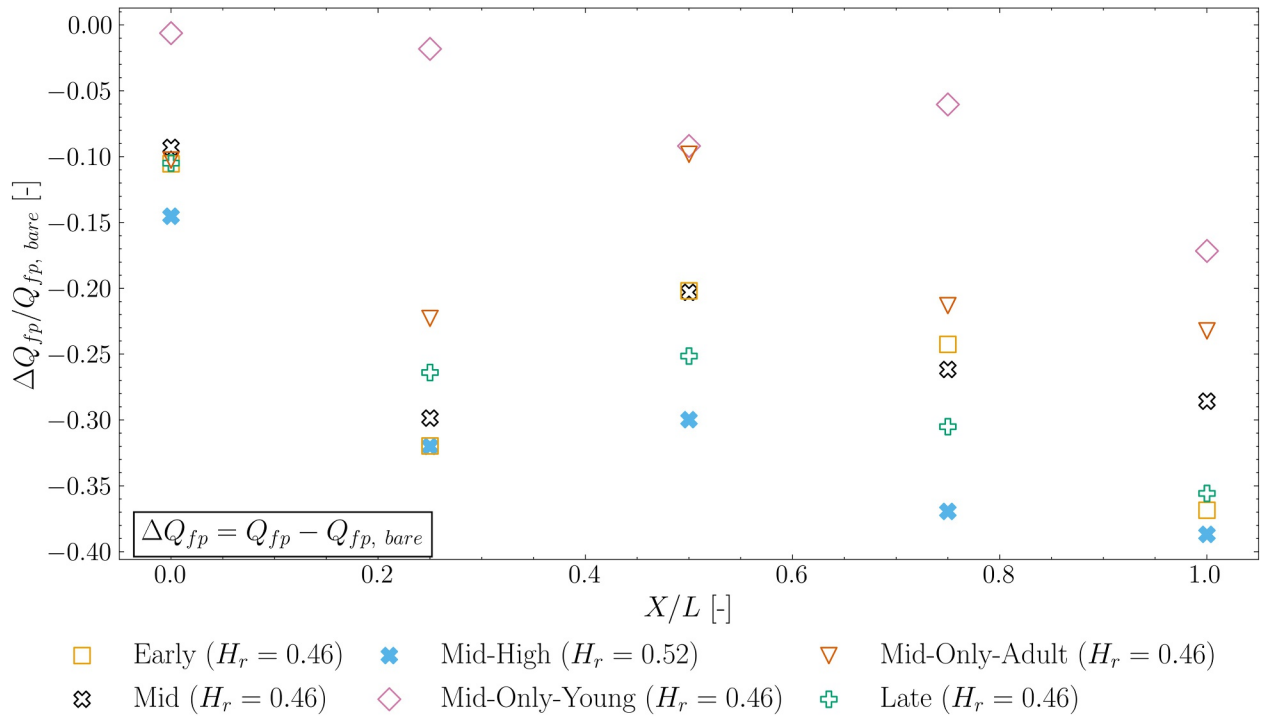

Figure 8. Longitudinal distribution of the floodplain discharge deviation from the reference cases ($\Delta Q_{\mathrm{fp}} = Q_{\mathrm{fp}} - Q_{\mathrm{fp,bare}}$).

$$\tau_{\mathrm{xy}} = \frac{1}{H}\int_0^H -\rho u_x u_y \mathrm{d}z = -\rho\left(\overline{u_x' u_y'}\right)^{\mathrm{DA}} - \rho u_x^{\mathrm{DA}} u_y^{\mathrm{DA}} - \rho\left[u_x\left(u_y - u_y^{\mathrm{DA}}\right)\right]^{\mathrm{DA}} \quad (8)$$

According to Equation 8, the transversal flux τ_{xy} is split into three main components of: (a) transverse Reynolds stresses ($-\rho\left(\overline{u_x' u_y'}\right)^{\mathrm{DA}}$); (b) mean transverse flows ($-\rho u_x^{\mathrm{DA}} u_y^{\mathrm{DA}}$) and (c) secondary currents ($-\rho\left[u_x\left(u_y - u_y^{\mathrm{DA}}\right)\right]^{\mathrm{DA}}$).

Figure 9 shows the longitudinal evolution of the fluxes of total momentum and its components, between the main channel and the floodplain at the mixing layer center Y_c. In the Bare and *Bare-High* scenarios, the total momentum flux (τ_{xy}) was low due to the absence of mean transverse flow, as a consequence the Reynolds stresses and secondary currents became the main contributors. For compound channels with an inclined cross-section, the secondary flow magnitude is reduced compared to 90° (Barman & Kumar, 2023; Xiao et al., 2018), this combined with the Reynolds shear stress reduction of high relative water depth H_r (Proust et al., 2017; Stocchino & Brocchini, 2010) contributed to the low values of momentum flux. The forest introduction increased the total momentum flux by one order of magnitude when compared to Bare conditions. This increase was a consequence of the mean transverse flow u_y^{DA}, which became the main contributor, representing more than 95% of the total momentum, in agreement with Proust et al. (2013, 2017) and Proust and Nikora (2020). Once the flow readjusted, the contribution of the turbulence and secondary currents increased. In the last cross-section, the change in the mean transverse flow direction in the Early, Mid and Late scenarios, led to a momentum flux from the main channel toward the floodplain. The relative water depth H_r intensity led to higher values of momentum, due to a faster flow in both directions (u_x^{DA}, u_y^{DA}), which directly affected the mean transverse flows ($-\rho u_x^{\mathrm{DA}} u_y^{\mathrm{DA}}$), the main contributor for momentum exchange.

4.8. Solute Tracer Dispersion

Figure 10 shows the time-averaged tracer concentration for the experiments with the Mid age forest under intermediate flow conditions. Similar observations regarding tracer cloud width and dispersion were made under both intermediate and deep flow conditions. The tracer cloud width (W_{tracer}) was determined from the time-averaged tracer concentration using a color threshold to delineate the extent of the tracer cloud (Table 6). For

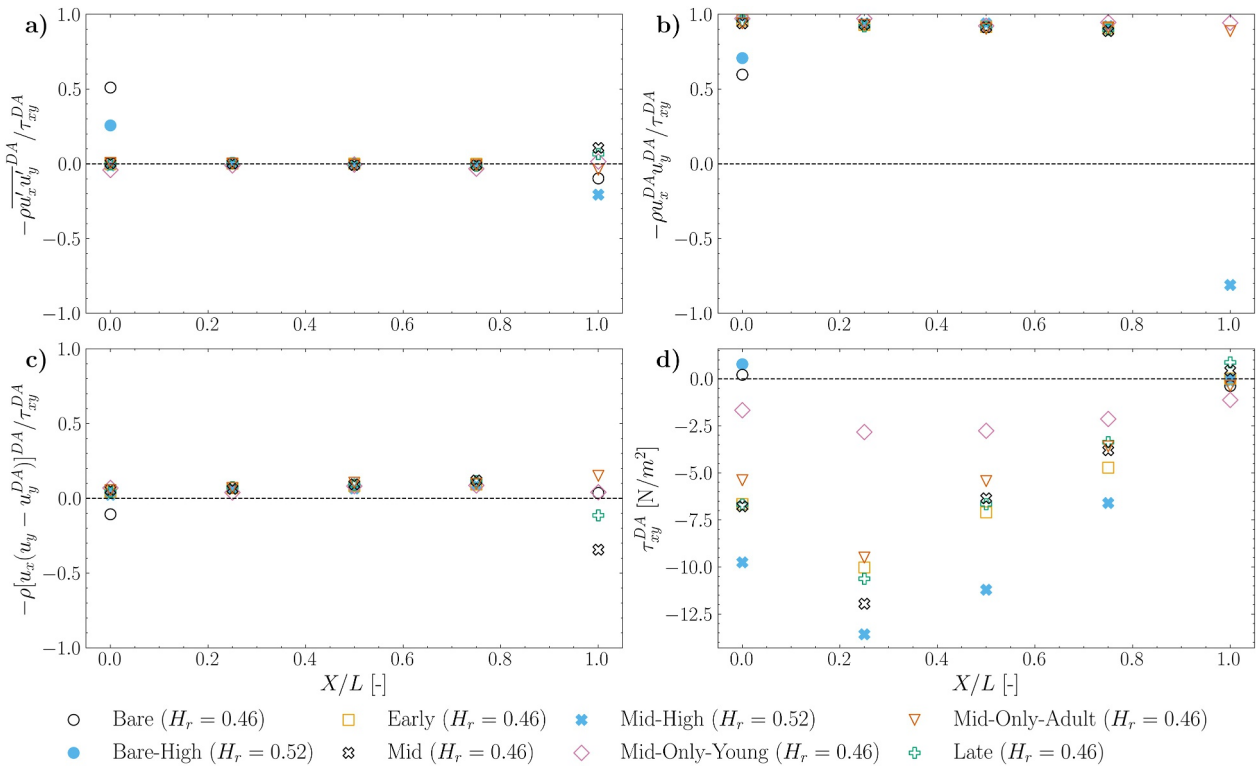

Figure 9. Longitudinal distribution of the momentum fluxes and its main contributors: (a) turbulence ($-\rho\left(\overline{u_x' u_y'}\right)^{\mathrm{DA}}$), (b) mean transverse flow ($-\rho u_x^{\mathrm{DA}} u_y^{\mathrm{DA}}$), (c) secondary currents ($-\rho\left[u_x\left(u_y - u_y^{\mathrm{DA}}\right)\right]^{\mathrm{DA}}$) and (d) the total depth-averaged streamwise momentum exchange at the *XY*-plane. Data at the mixing layer center (Y_c).

injection points located in the floodplain at $Y/W_{\mathrm{mc}} = -2.50$, the forest expanded the tracer cloud width. This expansion results from the combined effects of vegetation-induced diffusion and turbulence (Farzadkhoo et al., 2019; Nepf, 1999), and was more pronounced within the forest patch. In the transition region, the tracer cloud was advected laterally by the mean transverse flow. Flow acceleration in both the transition zone and the main channel led to narrower tracer clouds, consistent with Shiono et al. (2003), Hamidifar et al. (2015), and Farzadkhoo et al. (2019). Longitudinally, the tracer cloud widened in the floodplain and near the geometrical interface ($Y/W_{\mathrm{mc}} = 0.00$), while showing no significant growth at the mixing layer center (Y_c) or in the main channel ($Y/W_{\mathrm{mc}} = 1.48$). This pattern reflects vegetation-induced dissipation that enhances mixing within the forested region but is absent in the transition and main channel zones, resulting in a wider tracer cloud in the floodplain and a narrower one in the main channel. The flood intensity increase did not affect tracer cloud width in the main channel, as the fast flow limited lateral dispersion in both cases. In contrast, the effects of flood intensity were evident in the floodplain, where higher discharge accelerated the flow and reduced the time available for dispersion. In the *Mid-High* scenario, the faster floodplain flow produced a slightly narrower tracer cloud compared to the Mid scenario, consistent with Hamidifar et al. (2015), and Farzadkhoo et al. (2019).

5. Discussion and Practical Implications

5.1. Forest Age, Management and Hydrodynamics

We conducted experiments in a laboratory scale compound channel to investigate the effects of (a) vegetation aging, (b) forest management, and (c) the flow-depth ratio between the water depth in the floodplain (FP) and the main channel (MC), in the hydrodynamics of compound channels under flooding conditions. Overall, the Mid age forest had the highest deviation from the Bare conditions in terms of velocity, depth, and hydraulic parameters. This is attributed to the Mid age forest having the highest hydrodynamic density (*mD*, related to adult trees) value (Table 3), which proved to be dominant over the leaf area index (LAI, related to young trees) and solid volume fraction (ϕ, total density) metrics. Additionally, the Mid age forest had more elements (young and adult trees) than the other forest ages.

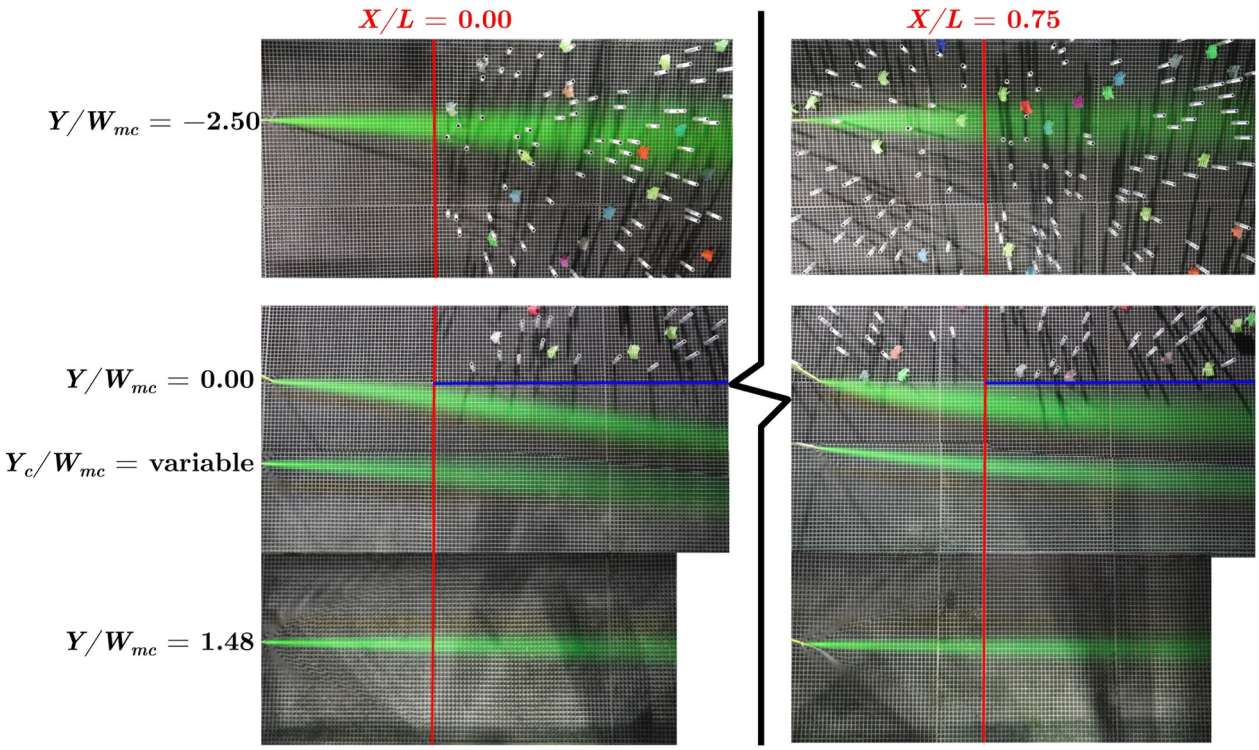

Figure 10. Time-averaged tracer concentration for the experiments representing the Mid age floodplain forest and for the relative flow depth, $H_r = 0.46$ at $X/L = 0.00$ and 0.75. The red line indicates the velocity measuring cross-sectional position which is located one m from the injection point, and the blue line indicates the geometrical interface at $Y/W_{mc} = 0$.

The velocity patterns inside the floodplain were affected by the placement of vegetation, producing local effects due to its presence or absence. These local effects impose challenges to the channel division proposed by Truong and Uijttewaal (2019) and the fit of analytical solutions (Fernandes et al., 2014; Shiono & Knight, 1991). Therefore, a simplified model based on the Unified-Richards function is proposed to describe the mean flow inside the vegetated zone and allow the division of the channel, while accounting for the shear asymmetry at the interface between floodplain and main channel (Figure 5). Overall, forest aging decreased the dimensionless shear λ; however, its value remained higher than that observed under Bare conditions. Similarly, the dimensionless shear decreased in forest management scenarios, due to lower vegetation density, and in flood intensity scenarios, which are associated with an increase in the relative water depth H_r.

The floodplain forest generated a mean transverse flow as the flow adjusted to the change in roughness. Forest aging affected both the peak magnitude of this transverse flow and the rate at which it decelerated as the flow

Table 6
Summary of the Tracer Cloud Dispersion at X/L = 0.00 and 0.75

Case	H_r [−]	Age	Y/W_{mc} [−]	W_{tracer} at $X/L = 0.00$ [−]	W_{tracer} at $X/L = 0.75$ [−]
3	0.46	Mid	−2.50	0.17	0.25
3	0.46	Mid	0.00	0.12	0.19
3	0.46	Mid	Y_c	0.12	0.10
3	0.46	Mid	1.48	0.07	0.07
8	0.52	Mid-High	−2.50	0.14	0.22
8	0.52	Mid-High	0.00	0.13	0.15
8	0.52	Mid-High	Y_c	0.12	0.11
8	0.52	Mid-High	1.48	0.07	0.08

readjusted. In the Mid and Late forest ages, higher peaks were observed, which can be associated with a higher hydrodynamic density (mD) values. Additionally, forest aging shortened the flow readjustment length, in line with an increase in total forest density, expressed by the solid volume fraction (ϕ), consistent with Rominger and Nepf (2011). This effect dominated over the change in adult tree density, expressed by the hydrodynamic density (mD), which initially increased and later decreased, as well as the decrease in young tree density indicated by the leaf area index (LAI). Forest management results indicated that adult trees contributed most significantly to the mean transverse flow due to their higher proportion and blockage (ϕ). Furthermore, higher flood intensity increased the mean transverse flow peak by 22% compared to intermediate flow conditions.

The water depth was affected by the forest in all regions of the flow (floodplain, main channel, and transition), with an increase in the upstream followed by a gradual decrease to values below Bare conditions. Forest aging led to changes of approximately 1.3% in flow depth within both measurement positions in the floodplain, with the maximum at Mid age. This highlights the importance of forest management as the increased water depth upstream lead to slower velocities and thus sedimentation and the acceleration downstream lead the bed propense to erosion (Havinga et al., 2009). Forest management practices, such as the removal of young trees, could reduce upstream flood risk, without significantly affecting downstream risk (Figure 8). However, a similar benefit could likely be achieved by removing shrubs that also occupy the submerged layer, without affecting the economic value of young trees associated with timber production. Furthermore, for a higher relative flow depth H_r the downstream effect and the length required for water depth recovery reduced. Lastly, forest aging should be considered when planning the installation of forest patches for downstream flood protection, determining the length of the reduced water depths and the increase of upstream depths.

The effects on the mixing layer were varied. Although its center position and center velocity remained largely unchanged, both its total width and the extent of its penetration into the floodplain were affected. Overall, forest vegetation widened the mixing layer, causing a portion of it to extend over the floodplain, not observed under Bare conditions, where the mixing layer was narrower. The mixing layer extent over the floodplain might have implications on sediment transport, as it affects the turbulent induced sediment transport, associated with macro-vortices in the mixing layer (Branß et al., 2022). Forest aging narrowed the mixing layer and reduced its proportional coverage over the floodplain, which was attributed to the reduction in the leaf area index (LAI). Furthermore, although both forest management scenarios yielded similar overall widths, their internal distributions differed: the inner mixing layer was wider in the *Mid-Only-Adult* scenario, whereas the outer layer was broader in the *Mid-Only-Young* scenario. The increase in flood intensity narrowed the mixing layer width due to a decrease in the dimensionless shear, which led to smaller floodplain penetration in the *Mid-High* case compared to the Mid age.

The forest induced an advective mass flux toward the main channel during flow readjustment, affecting sectional discharge and, consequently, mass transport. Forest aging reduced the forest's effect on mass exchange from 42% to 28%, and forest management further diminished this effect. The *Mid-Only-Adult* and Late scenarios exhibited similar discharge distributions, suggesting that the removal of young trees may reduce lateral mass exchange. This *Mid-Only-Adult* mass exchange reduction could affect floodplain soil conservation and the remobilization of heavy metals associated with sediments (Ciszewski & Grygar, 2016). Nonetheless, forest aging and soil's hydraulic conductivity are directly related due to the higher proportion and connectivity of macropores (Archer et al., 2016), which may increase aquifer recharge rates. This should be accounted for in river management. Furthermore, increasing flood intensity did not affect mass exchange, as similar values of floodplain flow discharge change ($\Delta Q_{\mathrm{fp}}/Q_{\mathrm{bare}}$) were observed in both the Mid and *Mid-High* scenarios.

Momentum exchange was primarily influenced by the mean transverse flow. Consequently, the introduction of forest vegetation resulted in an order-of-magnitude increase compared to Bare conditions. Moreover, momentum exchange was directly proportional to the relative water depth, as this parameter directly affects the mean transverse flows ($-\rho u_x^{\mathrm{DA}} u_y^{\mathrm{DA}}$), which serve as the main contributor to momentum exchange.

Tracer dispersion was strongly influenced by vegetation and discharge conditions. Injections within the floodplain ($Y/W_{\mathrm{mc}} = -2.50$) produced wider tracer clouds due to vegetation-induced diffusion and turbulence (Farzadkhoo et al., 2019; Nepf, 1999), while at the floodplain–main channel interface ($Y/W_{\mathrm{mc}} = 0.00$) the effect was weaker but still noticeable. In contrast, dispersion at the mixing layer center (Y_c) and in the main channel ($Y/W_{\mathrm{mc}} = 1.48$) remained nearly unchanged, reflecting advection-dominated transport in faster flows, consistent

with observations by Shiono et al. (2003), Hamidifar et al. (2015), and Farzadkhoo et al. (2019). In these regions, the tracer cloud was advected laterally following the direction of the mean transverse flow. Increasing discharge from Mid to *Mid-High* conditions did not affect the main channel but reduced cloud width in the floodplain, as higher velocities shorten the residence time available for mixing and thus limits dispersion (Farzadkhoo et al., 2019; Hamidifar et al., 2015). These findings suggest that flood intensity, together with vegetation, regulates solute diffusion and longitudinal transport in the floodplain.

The results and conclusions presented here are only valid for flows in straight compound channels under steady flow conditions. These findings were derived from experiments conducted at high relative water depths, which may differ under shallower conditions. Additionally, only one vegetation patch length was used in the channel, as opposed to vegetation covering the entire floodplain longitudinally or using different patch lengths.

5.2. Flood Risk Mitigation and Navigability

Flood risk and navigation are intrinsically interconnected (Middelkoop et al., 2004), as rivers must continue to fulfill their social, ecological and economic functions. Therefore, river interventions should aim to mitigate flood risk while preserving main channel navigability, biodiversity, and the associated ecosystem services. On flood risk, the forest increased the upstream water depth up to +8% when compared to Bare conditions. For downstream the forest, the flood risk decreased up to −2%. Forest aging produced changes in water depth of up to 1.3% both upstream and downstream in the floodplain. In the main channel, forest aging did not result in significant changes. In terms of forest management, the *Mid-Only-Young* scenario was most effective in reducing upstream risk by 4%, although it increased downstream risk. This implies that vegetation removal might be beneficial when the forest is located downstream of an urban area, yet such management could increase risk if the forest is upstream. However, under natural conditions, forests enhance water infiltration, rainfall interception, and transpiration (Bentley & Coomes, 2020; Wittmann et al., 2022), which in turn influence flood risk but could not be represented in our experiments.

From a navigational perspective, water depth changes induced by the forest in the main channel were lower than those in the floodplain, ranging from −0.5% downstream to 2% upstream. The longitudinal water depth effect was similar across all forest age cases, particularly in the downstream section, where water depth recovery extended for approximately 1.5 times the forest length, directly impacting bridge clearance. The presence of floodplain forest, compared to Bare conditions, enhanced flow cross-sectional heterogeneity during flood events. This increased heterogeneity may reduce the risk of main channel shoal formation, as floodplains, among other ecosystem services, retain sediments (Juez et al., 2019; Västilä & Jilbert, 2025). Combined, these observations should inform river managers in the design of floodplain interventions and the placement of floodplain reactivation projects, potentially reducing river stakeholder conflicts.

5.3. Hydraulic Modeling

Numerical models are important tools for assessing flood risk and its management, as well as for investigating mass and momentum exchanges. In this section, we show the impact of forest aging on hydraulic modeling, where the division between the main channel and floodplain was geometrically set at $Y/W_{\mathrm{mc}} = 0$. This division was adopted to facilitate the application of the section in numerical models, as the mixing layer center is not a fixed position. Throughout the forest ages, the value of the hydraulic radius ($R_h = A_{f,i}/P_{w,i}$, where $P_{w,i}$ is the wetted perimeter) was constant, with $R_h = 0.11$ m (intermediate flow) and $R_h = 0.13$ m (deep flow). The effects on the hydraulic roughness were investigated with the Strickler coefficient, k_{st} (Equation 9).

$$k_{\mathrm{st}} = \frac{\ddot{u}_x}{R_h^{2/3} \cdot \sqrt{\sin S_0}} \tag{9}$$

where, S_0 [−] is the longitudinal channel bed slope.

The effect of flow non-uniformity across the section was investigated using the velocity correction coefficients: the energy (Coriolis) coefficient α (Equation 10) and the momentum (Boussinesq) coefficient β (Equation 11).

Table 7
Summary of the Depth and Transversal Averaged Hydraulic Modeling Parameters for the Measuring Section at X/L = 1.00

Case	H_r [−]	Age	k_{st} [$m^{1/3}$ s^{-1}]	$k_{st,mc}$ [$m^{1/3}$ s^{-1}]	$k_{st,fp}$ [$m^{1/3}$ s^{-1}]	α [−]	α_{mc} [−]	α_{fp} [−]	β [−]	β_{mc} [−]	β_{fp} [−]	τ_a [N/m^2]
1	0.46	Bare	47.9	52.1	48.2	2.93	1.24	1.30	1.66	1.10	1.13	0.13
2	0.46	Early	40.7	62.0	27.8	4.62	1.28	1.68	2.02	1.11	1.27	0.15
3	0.46	Mid	43.6	62.3	32.8	4.27	1.29	1.40	1.94	1.12	1.16	0.16
4	0.46	Late	44.5	62.0	34.7	4.07	1.27	1.42	1.90	1.11	1.17	−0.17
5	0.46	Mid-Only-Young	47.4	55.6	45.0	3.17	1.24	1.35	1.71	1.10	1.15	0.39
6	0.46	Mid-Only-Adult	44.6	60.8	35.7	3.96	1.28	1.33	1.87	1.11	1.14	0.24
7	0.52	Bare-High	55.2	57.5	56.5	2.18	1.19	1.19	1.44	1.08	1.08	0.27
8	0.52	Mid-High	49.4	69.9	38.2	3.34	1.24	1.23	1.70	1.10	1.10	0.42

Note. The data in this table was scaled into field conditions and measured at $Y = 0$.

$$\alpha = \frac{\int_A u_x^3 \cdot dA}{U_x^3 \cdot A_{f,i}} \tag{10}$$

$$\beta = \frac{\int_A u_x^2 \cdot dA}{U_x^2 \cdot A_{f,i}} \tag{11}$$

The apparent shear stress between the main channel and floodplain was calculated with Equation 12, which provides a partition of the apparent shear stress into the Reynolds shear stress and the transverse flow stress (Fernandes, 2021; Shiono & Knight, 1991).

$$\tau_a = -\rho \cdot \overline{u_x' u_y'} + \rho \cdot u_x^{DA} u_y^{DA} \tag{12}$$

The influence of the floodplain forests on the cross-sectional averaged values of the Strickler coefficients, velocity corrector coefficients, and apparent shear stress are shown in Table 7. Overall, vegetated scenarios exhibited increased hydraulic roughness and greater flow non-uniformity compared to Bare conditions. Consistent with Keshavarzi and Hamidifar (2018) and Hamidifar et al. (2016), the energy coefficient was higher than the momentum coefficient. Forest aging reduced hydraulic roughness by 9%, the energy correction coefficient by 11%, and the momentum correction coefficient by 6%, when comparing the Early and Late stages. Moreover, forest management reduced hydraulic roughness and both velocity correction coefficients, as a result of decreased blockage. In the *Mid-Only-Adult* scenario, hydraulic roughness was similar to that of the Late stage, despite the latter exhibiting a twofold higher solid volume fraction and a two-layered vegetation configuration. Additionally, increased flood intensity reduced both roughness and flow non-uniformity, exerting a greater influence than either forest aging or forest management.

The sub-sectionally averaged values of the Strickler coefficients and velocity corrector coefficients were analyzed (Table 7). Overall, the floodplain exhibited higher roughness compared to the main channel, while the velocity correction coefficients were higher in the floodplain. The floodplain forest further increased floodplain roughness, which in turn led to a smoother main channel as more flow was conveyed in this region. Conversely, while the floodplain exhibited a more non-uniform flow, the flow in the main channel the velocity corrector coefficients were less affected and kept a similar magnitude as in the Bare scenarios. Forest aging did not significantly alter the hydraulic conditions in the main channel, but the floodplain became 25% hydraulically smoother, and with a more uniform flow when comparing the Early and Late ages. Forest management generally mitigated the effects observed in the Mid age; however, unlike cross-sectional averaged hydraulic roughness values, the *Mid-Only-Adult* case did not resemble the Late age. Finally, increased flood intensity reduced both overall roughness and flow non-uniformity, an observation that is consistent with the main channel smoothing reported by Naghavi et al. (2022), in a meandering compound channel.

The apparent shear stress typically required in coupled (1D–1D or 1D–2D) models and for discharge calculations is shown in Table 7. Discharge estimation cannot be performed directly using the hydraulic radius R_h, the fluid-fluid interface between regions cannot be captured; thus, an apparent shear stress (τ_a) is needed to represent this interface (Fernandes, 2021; Moreta & Martin-Vide, 2010; Myers, 1978; Shiono & Knight, 1991). The primary contribution was from the mean transverse flow ($-\rho \cdot u_x^{\mathrm{DA}} u_y^{\mathrm{DA}}$), when compared to the Reynolds stresses. The presence of floodplain forest increased the magnitude of the apparent shear stress compared to the Bare scenario. While forest aging did not significantly change the apparent shear stress magnitude overall, an inverted sign was observed in the Late age, which was attributed to the inversion of the mean transverse flow velocity (Figure S4 in Supporting Information S1). Additionally, forest management further increased the apparent shear stress, with the *Mid-Only-Young* scenario exhibiting higher values due to the longer persistence of non-zero mean transverse flow velocities. Flood intensity led to an 111% increase in the apparent shear stress in the *Bare-High* scenario and a 159% increase in the *Mid-High* scenario.

Our data were also compared to literature models, such as the apparent shear stress model (Moreta & Martin-Vide, 2010), and the discharge model based on apparent shear stress (Fernandes, 2021). We found that the apparent shear stress model was unable to accurately predict the apparent shear stress, a shortcoming attributed to the flow heterogeneity over the floodplain and the presence of a mean transverse flow. Under Bare conditions, the model exhibited a relative difference of −186% for intermediate flows, which decreased to 6% for deep flows where the channel was hydraulically smoother (Table 5). For the discharge model based on apparent shear stress, the discharge was calculated as:

$$Q_{\mathrm{mc}} = A_{f,\mathrm{mc}} \cdot R_{h\,\mathrm{mc}}^{2/3} \cdot k_{st,\mathrm{mc}} \cdot S_0^{1/2} \sqrt{1 - \left(\frac{N_{\mathrm{fp}} \cdot \tau_a \cdot H_{\mathrm{fp}}}{\rho \cdot g \cdot A_{\mathrm{mc}} \cdot S_0}\right)} \tag{13}$$

$$Q_{\mathrm{fp}} = A_{f,\mathrm{fp}} \cdot R_{h\,\mathrm{fp}}^{2/3} \cdot k_{st,\mathrm{fp}} \cdot S_0^{1/2} \sqrt{1 + \left(\frac{\tau_a \cdot H_{\mathrm{fp}}}{\rho \cdot g \cdot A_{\mathrm{fp}} \cdot S_0}\right)} \tag{14}$$

where, N_{fp} [−] is the number of floodplains.

The performance of the discharge model was directly linked to the presence of a mean transverse flow. Under Bare conditions at the most downstream cross-section, the model was accurate with an error between 5% and 6%. However, in cross-sections with significant mean transverse flow, the model failed to accurately estimate discharge—underestimating it in the main channel while overestimating it in the floodplain. This discrepancy is attributable to the directional influence of the mean transverse flow and is likely to be reversed when the mean transverse flow is directed toward the floodplain.

In this paper, we presented forest-scale bulk values for parameters relevant to hydraulic modeling and examined how these parameters vary in response to floodplain forest succession, with vegetation effects being implicitly accounted for. The observed effects of floodplain forest succession on hydraulic roughness, velocity correction coefficients, and apparent shear stress could be usefully applied for 1D, 2D, and coupled 1D–1D or 1D–2D hydraulic modeling. However, it is recommended to employ models that explicitly incorporate vegetation effects, where vegetation roughness is decomposed and varies in response to the flow (Box et al., 2022; Folke et al., 2019).

5.4. Flow Zones and Lateral Connectivity

The forest induced a mean transverse flow that strongly influenced the hydrodynamics of the compound channel, as demonstrated in previous sections. Within the floodplain, this transverse flow was not uniform but instead divided into two distinct zones: one near the transition area exhibiting faster transverse flow, and another farther from the main channel where lateral flow was negligible. These contrasting regions created an energy deficit that affects mass and momentum exchanges as well as the development of the mixing layer. The low-energy area, referred to as the steady zone (orange area, Figure 11), is likely prone to higher sedimentation levels due to vegetation drag (Juez et al., 2019), potentially acting as a depositional zone. In contrast, the high-energy region with faster transverse flow, the divergence zone (blue area, Figure 11), tends to experience lower sedimentation

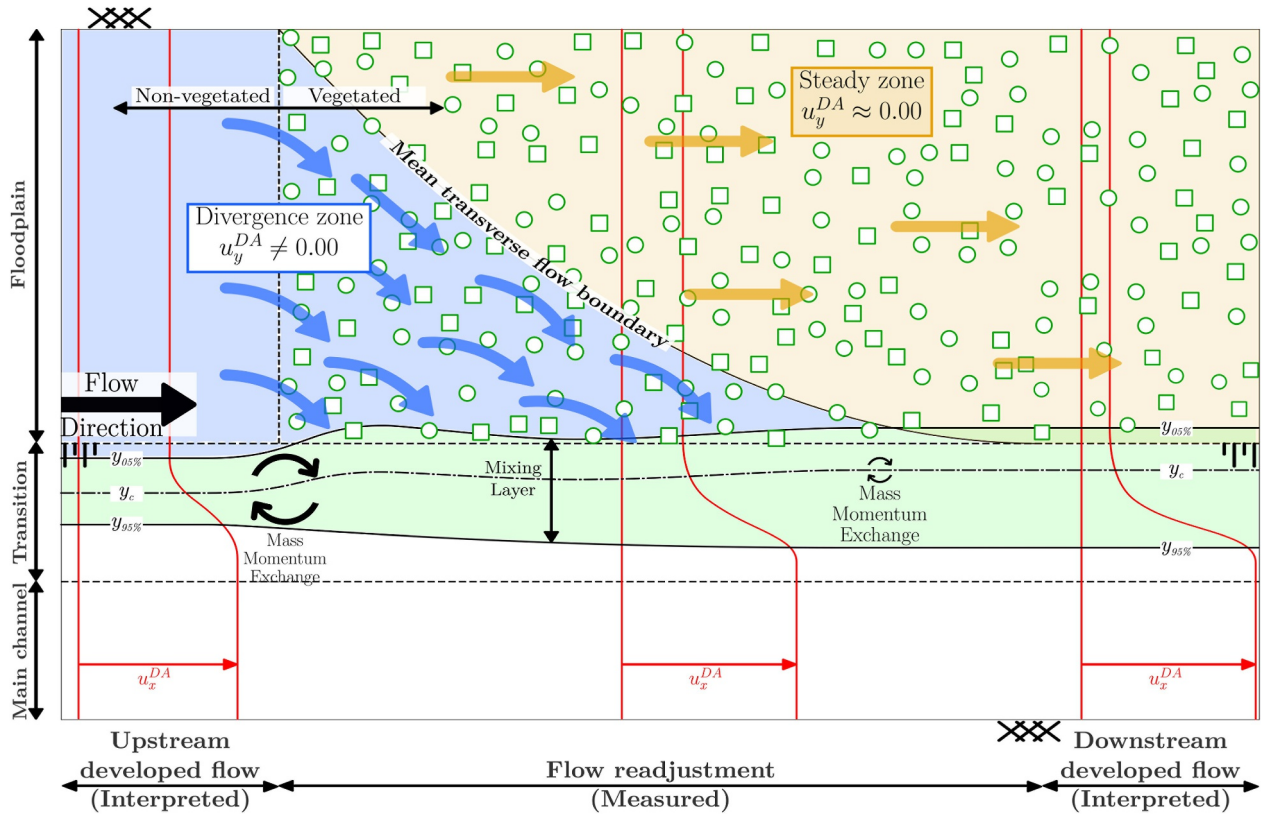

Figure 11. Sketch of the flow development in the transition of a non-vegetated to a vegetated floodplain in compound channel flow: identification of flow regions and the influence of the forest induced mean transverse flow on the flow development, mixing layer characteristics and position, and the lateral exchanges of mass and momentum.

rates since most of the water is diverted into the main channel. This flow divergence enhances mass and momentum exchange rates from the floodplain toward the main channel (Figures 8 and 9) and disrupts the quasi-uniform development of the mixing layer width typically observed under uniform conditions. The interplay between these zones may increase topographic complexity (White et al., 2023) and soil composition heterogeneities; as for instance, in the Upper Rhine River, floods serve as the primary source of phosphorus and nitrogen (Olde Venterink et al., 2006; Trémolières et al., 1998).

6. Conclusions

In this study, we conducted experiments on an asymmetric compound channel with varying floodplain forest ages and flow-depth ratios between the main channel (MC) and floodplain (FP). The forest characteristics, in this study, were based on a natural forest in the Upper Rhine, at a scale of 1:30. The main findings are listed below:

The effect of floodplain forest:

- Its spatial heterogeneity creates local velocity effects within the floodplain that challenge the usage of traditional analytical models. A regression model was developed to describe the depth-averaged cross-sectional profile of the streamwise velocity. The model allows for the analytical calculation of the internal and external mixing layer widths independently, the maximum lateral gradient of the streamwise velocity and its position. Our proposed model had a good performance, under uniform and non-uniform conditions, with a fit of $R^2 = 0.85$–0.99 and RMSE/U = 2.5%–14.4%.
- Vegetation enhanced tracer dispersion in the floodplain and at the channel–floodplain interface, while dispersion in the main channel remained limited under advection-dominated conditions.

The effect of forest aging is threefold:

- Forest aging decreases, due to a reduction in the reduction in the leaf area index (LAI), the velocity difference between the floodplain and main channel, as the main channel observed similar velocities, while the floodplain flow accelerated. This leads to a decrease in the dimensionless shear and a narrowing of the mixing layer.
- For hydraulic modeling, forest aging does not affect the main channel's hydrodynamic roughness or velocity correction coefficients. However, it smooths both the floodplain and cross-sectional regions, leading to more uniform flow conditions.
- Forest aging also reduces lateral mass exchange between the main channel and floodplain and alters lateral momentum exchange, which was primarily governed by the mean transverse flow.

On the forest management effect:

- Selective tree removal can reduce the upstream backwater effect, without significantly changing the downstream water depth reduction.
- The young trees removal, in the *Mid-Only-Adult* scenario, showed similar discharge and hydraulic roughness conditions as the Late age. Showing an artificial aging effect on hydrodynamics.

Flood intensity effects on vegetated compound channels:

- Flood intensity governs the magnitude of lateral flow readjustment, exerting a positive feedback on the peak mean transverse velocity, peak backwater effect, and lateral discharge distribution, while exerting a negative feedback on the dimensionless shear and mixing layer width.
- From a hydraulic modeling perspective, increasing flood intensity amplifies apparent shear stress, reduces velocity correction coefficients, and results in hydraulically smoother conditions.
- For intermediate and deep flow conditions, flood intensity increase did not affect tracer cloud width in the main channel but reduced dispersion in the floodplain, resulting in a narrower cloud.

The findings presented here can assist managers and engineers in anticipating challenges due to forest aging and maintaining designed functions, by providing the effects to hydraulic models, forest patch effects on water depth aiding the positioning of floodplain reactivation projects and the development of a model to describe the flow profile under uniform and non-uniform conditions. Further research should consider flow unsteadiness, which is correlated with changes in dimensionless shear, lateral exchanges, stresses, velocity distributions, and hyporheic flow (Kaddi et al., 2024; Liu et al., 2024a, 2024b; Xiao et al., 2022). Variations in forest length may also impact the flow readjustment length (Rominger & Nepf, 2011), while vegetation randomization influences background turbulence and turbulent kinetic energy (Ricardo et al., 2014, 2016, 2018) and must be further explored. Lastly, the influence of a mobile bed should be investigated, as its omission may lead to an overestimation of vegetation effects (Branß & Aberle, 2022).

Notations

$\tilde{u}_x$	Sub-section time- and spatially averaged streamwise velocity
A	Surveyed forest area
A_B	Ground area of the silicon element representing the young trees
$A_{f,\mathrm{fp}}$, $A_{f,\mathrm{mc}}$	Flow area in the floodplain, and main channel
A_L	One-sided leaf area
B	Tree basal area in the surveyed forest
d	Parameter that controls the asymmetry in the Unified-Richards equation
D_r	Cylinder diameter representing an adult tree
D_t	Trunk diameter at breast height
Fr	Froude number
g	Gravitational acceleration

H_{fp}, H_{mc}	Flow depth in the floodplain, and main channel
H_r	Relative flow depth
H_t	Tree height
H_{tr}	Geometrical transition height
k	Maximum value of the transversal depth-averaged velocity gradient
k_{st}	Strickler hydraulic roughness coefficient
L	Forest patch length
LAI	Leaf area index
mD	Hydrodynamic density
n, n_a, n_y	Number of trees per square meter of total, adult, and young trees
N_{fp}	Number of floodplains used in the discharge method based on the apparent shear stress
N_t, N_a, N_y	Number of total, adult and young trees
P_i	The proportion of trees in the field
$P_{w,i}$	Wetted perimeter
Q, Q_{mc}, Q_{fp}	Total, main channel and floodplain flow discharges
R_h	Hydraulic radius
Re	Reynolds number
S_0	Longitudinal channel bed slope
TKE	Turbulent kinetic energy
U	Bulk flow velocity
$u^{\text{DA}}_{x,\text{fp}}$	Mean depth averaged streamwise velocity in the floodplain
$u^{\text{DA}}_{x,\text{mc}}$	Maximum depth averaged streamwise velocity in the main channel
$u_{5\%}$, $u_{95\%}$	Inner and outer mixing layer depth-averaged boundary velocities
u^{DA}_c	Depth-averaged velocity at the center of the mixing layer
$\ddot{u}_i$	Geometrical subsection averaged velocity
u_m	Scaled velocity used to calculate the silicon elements reactive force
u_x, u_y, u_z	Streamwise, transversal and vertical instantaneous velocity
$\overline{u}_x$, $\overline{u}_y$, $\overline{u}_z$	Streamwise, transversal and vertical time-averaged velocity
u'_x, u'_y, u'_z	Streamwise, transverse and vertical velocity time fluctuation
u^{DA}_x, u^{DA}_y, u^{DA}_z	Time- and depth-averaged streamwise, transverse and vertical velocities
V_i	Single element volume
W_{fp}, W_{mc}, W_{tr}	Floodplain, main channel and transition widths
W_{tracer}	Tracer cloud width
X, Y, Z	Longitudinal, transverse and vertical coordinates
Y_c	Inflection point in the transversal depth-averaged streamwise velocity profile (mixing layer center)

α	Energy (Coriolis) velocity corrector
α_{rot}, β_{rot}, γ_{rot}	Vertical-axed, spanwise-axed and streamwise-axed adv rotation angles
β	Momentum (Boussinesq) velocity corrector
δ, δ_{in}, δ_{out}	Total, inner and outer mixing layer widths
ΔH	Water depth change (difference between vegetated and bare conditions)
Δu	Depth-averaged velocity difference between main channel and floodplain
λ	Dimensionless shear
ν	Kinematic viscosity
ρ	Water density
τ_a	Apparent shear stress
τ_{xy}	Total depth-averaged streamwise momentum flux in the *xy*-plane
ϕ	Solid volume fraction

Conflict of Interest

The authors declare no conflicts of interest relevant to this study.

Availability Statement

The data set underlying this study is available at the Federal Waterways Engineering and Research Institute (BAW) data repository via https://doi.org/10.48437/7baa8b-9fb1a0 (de Oliveira et al., 2026) with a CC BY 4.0 license (https://creativecommons.org/licenses/by/4.0/deed.en).

Acknowledgments
This research was conducted within the framework of the University of Naples Federico II (UNINA) Civil Systems Engineering PhD Program, which funded de Oliveira's stay at the Karlsruhe Institute of Technology (KIT) and the Federal Waterways Engineering and Research Institute (BAW). The present study was carried out under the financial supports from the Coordenação de Aperfeiçoamento de Pessoal de Nível Superior Brazil (CAPES) – Finance Code 001, CAPES - Institutional Internationalisation Programme (Print). This research was funded by Instituto Nacional de Ciência e Tecnologia em Soluções baseadas na Natureza—INCT "SbN" (INCT "Nature based Solutions"); CAPES; Conselho Nacional de Desenvolvimento Científico e Tecnológico (CNPq) - Brazil; and Fundação de Amparo à Pesquisa do Estado do Rio Grande do Sul (FAPERGS). Open Access funding enabled and organized by Projekt DEAL.

References

Aberle, J., & Järvelä, J. (2013). Flow resistance of emergent rigid and flexible floodplain vegetation. *Journal of Hydraulic Research*, *51*(1), 33–45. https://doi.org/10.1080/00221686.2012.754795

Ackers, P. (1993). Flow formulae for straight two-stage channels. *Journal of Hydraulic Research*, *31*(4), 509–531. https://doi.org/10.1080/00221689309498874

Archer, N. A. L., Otten, W., Schmidt, S., Bengough, A. G., Shah, N., & Bonell, M. (2016). Rainfall infiltration and soil hydrological characteristics below ancient forest, planted forest and grassland in a temperate northern climate. *Ecohydrology*, *9*(4), 585–600. https://doi.org/10.1002/eco.1658

Azevedo, R., Leal, J. B., & Rojas-Solórzano, L. (2012). Influence of vegetation on compound-channel turbulent field. In *River flow 2012*. Murillo.

Barman, J., & Kumar, B. (2022). Flow behaviour in a multi-layered vegetated floodplain region of a compound channel. *Ecohydrology*, *15*(4), e2427. https://doi.org/10.1002/eco.2427

Barman, J., & Kumar, B. (2023). Flow in multi-layered vegetated compound channels with different bank slopes. *Physics of Fluids*, *35*(3), 036601. https://doi.org/10.1063/5.0142400

Bentley, L., & Coomes, D. A. (2020). Partial river flow recovery with forest age is rare in the decades following establishment. *Global Change Biology*, *26*(3), 1458–1473. https://doi.org/10.1111/gcb.14954

Bernhardt, C. (2000). Die Rheinkorrektion. *Der Bürger Im Staat*, *50*, 76–81.

Bose, A. K., Schelhaas, M.-J., Mazerolle, M. J., & Bongers, F. (2014). Temperate forest development during secondary succession: Effects of soil, dominant species and management. *European Journal of Forest Research*, *133*(3), 511–523. https://doi.org/10.1007/s10342-014-0781-y

Box, W., Järvelä, J., & Västilä, K. (2022). New formulas addressing flow resistance of floodplain vegetation from emergent to submerged conditions. *International Journal of River Basin Management*, *22*(3), 1–17. https://doi.org/10.1080/15715124.2022.2143512

Branß, T., & Aberle, J. (2022). Combined effect of a mobile bed and floodplain edge vegetation on compound channel conveyance. *Journal of Hydraulic Research*, *60*(5), 826–834. https://doi.org/10.1080/00221686.2022.2041498

Branß, T., Núñez-González, F., & Aberle, J. (2022). Fluvial levees in compound channels: A review on formation processes and the impact of bedforms and vegetation. *Environmental Fluid Mechanics*, *22*(2–3), 559–585. https://doi.org/10.1007/s10652-022-09850-9

Brown, G. L., & Roshko, A. (1974). On density effects and large structure in turbulent mixing layers. *Journal of Fluid Mechanics*, *64*(4), 775–816. https://doi.org/10.1017/S002211207400190X

Burrows, C. J. (1991). *Processes of vegetation change*. Springer. https://doi.org/10.1007/978-94-011-3058-5

Caroppi, G., Västilä, K., Gualtieri, P., Järvelä, J., Giugni, M., & Rowiński, P. M. (2021). Comparison of flexible and rigid vegetation induced shear layers in partly vegetated channels. *Water Resources Research*, *57*(3), e2020WR028243. https://doi.org/10.1029/2020WR028243

Christensen, N. L., & Peet, R. K. (1984). Convergence during Secondary forest succession. *Journal of Ecology*, *72*(1), 25–36. https://doi.org/10.2307/2260004

Ciszewski, D., & Grygar, T. M. (2016). A review of flood-related storage and remobilization of heavy metal pollutants in river systems. *Water, Air, & Soil Pollution*, *227*(7), 239. https://doi.org/10.1007/s11270-016-2934-8

Crosato, A., & Saleh, M. S. (2011). Numerical study on the effects of floodplain vegetation on river planform style. *Earth Surface Processes and Landforms*, *36*(6), 711–720. https://doi.org/10.1002/esp.2088

de Oliveira, L. E. D., Janzen, J. G., Folke, F., Wittmann, F., Huber, N. P., Franca, M. J., & Gualtieri, C. (2026). Hydrodynamics of four moments in the life of a floodplain forest in compound channels [dataset]. *[Excel]. Federal Waterways Engineering and Research Institute (BAW): BAW-Datenrepository*. https://doi.org/10.48437/7baa8b-9fb1a0

Diaz-Redondo, M., Egger, G., Marchamalo, M., Hohensinner, S., & Dister, E. (2017). Benchmarking fluvial dynamics for process-based river restoration: The upper Rhine River (1816–2014). *River Research and Applications*, *33*(3), 403–414. https://doi.org/10.1002/rra.3077

Dister, E. (1980). *Geobotanische Untersuchungen in der hessischen Rheinaue als Grundlage für die Naturschutzarbeit*. University. G/Sttingen, RFA.

Dister, E., Gomer, D., Obrdlik, P., Petermann, P., & Schneider, E. (1990). Water mangement and ecological perspectives of the upper Rhine's floodplains. *Regulated Rivers: Research & Management*, *5*(1), 1–15. https://doi.org/10.1002/rrr.3450050102

Dupuis, V., Proust, S., Berni, C., & Paquier, A. (2017). Compound channel flow with a longitudinal transition in hydraulic roughness over the floodplains. *Environmental Fluid Mechanics*, *17*(5), 903–928. https://doi.org/10.1007/s10652-017-9525-0

Dupuis, V., Proust, S., Berni, C., & Paquier, A. (2017). Mixing layer development in compound channel flows with submerged and emergent rigid vegetation over the floodplains. *Experiments in Fluids*, *58*(4), 30. https://doi.org/10.1007/s00348-017-2319-9

Dupuis, V., Schraen, L., & Eiff, O. (2023). Shear layers in two-stage compound channels investigated with LS-PIV. *Experiments in Fluids*, *64*(2), 24. https://doi.org/10.1007/s00348-022-03557-9

Egler, F. E. (1954). Vegetation science concepts I. Initial floristic composition, a factor in old-field vegetation development with 2 figs. *Vegetatio*, *4*(6), 412–417. https://doi.org/10.1007/BF00275587

Farzadkhoo, M., Keshavarzi, A., Hamidifar, H., & Javan, M. (2019). Sudden pollutant discharge in vegetated compound meandering rivers. *Catena*, *182*, 104155. https://doi.org/10.1016/j.catena.2019.104155

Fernandes, J. N. (2021). Apparent roughness coefficient in overbank flows. *SN Applied Sciences*, *3*(7), 696. https://doi.org/10.1007/s42452-021-04677-3

Fernandes, J. N., Leal, J. B., & Cardoso, A. H. (2014). Improvement of the lateral distribution method based on the mixing layer theory. *Advances in Water Resources*, *69*, 159–167. https://doi.org/10.1016/j.advwatres.2014.04.003

Fernandes, J. N., Leal, J. B., & Cardoso, A. H. (2018). Influence of floodplain and riparian vegetation in the conveyance and structure of turbulent flow in compound channels. In *E3S Web of Conferences*, A. Paquier & N. Rivière (Eds.), River Flow 2018 (Vol. 40, p. 06035). https://doi.org/10.1051/e3sconf/20184006035

Folke, F. (2023). Abbildung der Rauheitswirkung von Vorlandvegetation in der ingenieurtechnischen Anwendung. *Universitätsbibliothek Braunschweig*. https://doi.org/10.24355/DBBS.084-202308221312-0

Folke, F., & Aberle, J. (2024). Hydraulic resistance of near-natural floodplain vegetation: A dataset for validating numerical models using a laboratory scale model. In *Presented at the 8th IAHR Europe Congress, Lisbon*.

Folke, F., Kopmann, R., Dalledonne, G., & Attieh, M. (2019). Comparison of different vegetation models using TELEMAC-2D. Retrieved from https://hdl.handle.net/20.500.11970/107161

Goring, D. G., & Nikora, V. I. (2002). Despiking acoustic Doppler velocimeter data. *Journal of Hydraulic Engineering*, *128*(1), 117–126. https://doi.org/10.1061/(ASCE)0733-9429(2002)128:1(117)

Hamidifar, H., Omid, M. H., & Keshavarzi, A. (2015). Longitudinal dispersion in waterways with vegetated floodplain. *Ecological Engineering*, *84*, 398–407. https://doi.org/10.1016/j.ecoleng.2015.09.048

Hamidifar, H., Omid, M. H., & Keshavarzi, A. (2016). Kinetic energy and momentum correction coefficients in straight compound channels with vegetated floodplain. *Journal of Hydrology*, *537*, 10–17. https://doi.org/10.1016/j.jhydrol.2016.03.024

Havinga, H., Schielen, R. M. J., & van Vuren, S. (2009). Tension between navigation, maintenance and safety calls for an integrated planning of flood protection measures. In *Proceedings of the 6th IAHR symposium on river, coastal and estuarine morphodynamics*. Santa Fé. Argentina.

Hu, R., & Zhang, J. (2022). Modeling velocity in a compound channel with co-existing emergent and submerged vegetation. *Physics of Fluids*, *34*(10), 105127. https://doi.org/10.1063/5.0121264

Hutter, B. (2018). *Abschätzung der oberirdischen Holzbiomasse und des Kohlenstoffspeichers in der Rastatter Rheinaue (Bsc-Thesis in Geoecology)*. Institute for Geographie and Geoecology. Karlsruhe Institute for Technology.

Johnson, E. A., & Miyanishi, K. (2007). *Plant disturbance ecology: The process and the response*. Elsevier/AP.

Johnson, T. E., Mcnair, J. N., Srivastava, P., & Hart, D. D. (2007). Stream ecosystem responses to spatially variable land cover: An empirically based model for developing riparian restoration strategies. *Freshwater Biology*, *52*(4), 680–695. https://doi.org/10.1111/j.1365-2427.2007.01726.x

Juez, C., Schärer, C., Jenny, H., Schleiss, A. J., & Franca, M. J. (2019). Floodplain land cover and flow hydrodynamic control of overbank sedimentation in compound channel flows. *Water Resources Research*, *55*(11), 9072–9091. https://doi.org/10.1029/2019WR024989

Kaddi, Y., Proust, S., Faure, J.-B., & Cierco, F.-X. (2024). Experimental and numerical study of unsteady flows in a compound open channel. *Environmental Fluid Mechanics*, *24*(3), 335–365. https://doi.org/10.1007/s10652-024-09988-8

Keshavarzi, A., & Hamidifar, H. (2018). Kinetic energy and momentum correction coefficients in compound open channels. *Natural Hazards*, *92*(3), 1859–1869. https://doi.org/10.1007/s11069-018-3285-0

Lightbody, A. F., Kui, L., Stella, J. C., Skorko, K. W., Bywater-Reyes, S., & Wilcox, A. C. (2019). Riparian vegetation and sediment supply regulate the morphodynamic response of an experimental stream to floods. *Frontiers in Environmental Science*, *7*, 40. https://doi.org/10.3389/fenvs.2019.00040

Liu, J., Xiao, Y., Xin, P., Wang, N., Yuan, S., Zhang, T., et al. (2024). Hyporheic exchange in a compound channel under unsteady flow: Numerical simulations. *Journal of Hydrology*, *631*, 130676. https://doi.org/10.1016/j.jhydrol.2024.130676

Liu, J., Xiao, Y., Zhou, J., Lin, Q., Yuan, S., Zhang, T., et al. (2024). Unsteady flow in a compound channel during flooding: Insights from a combined two-dimensional and three-dimensional numerical simulation. *Physics of Fluids*, *36*(8), 085124. https://doi.org/10.1063/5.0216832

LUBW. (2024). Hydrologische Landespegel—Daten-und Kartendienst [Dataset]. Retrieved from https://udo.lubw.baden-wuerttemberg.de/public/processingChain?repositoryItemGlobalId=hydrologische_landespegel&conditionValuesSetHash=F8CB46E&selector=hydrologische_landespegel&sourceOrderAsc=false&offset=0&limit=2147483647

Mera, I., Franca, M. J., Anta, J., & Peña, E. (2015). Turbulence anisotropy in a compound meandering channel with different submergence conditions. *Advances in Water Resources*, *81*, 142–151. https://doi.org/10.1016/j.advwatres.2014.10.012

Middelkoop, H., Van Asselt, M. B. A., Van' Klooster, T. S. A., Van Deursen, W. P. A., Kwadijk, J. C. J., & Buiteveld, H. (2004). Perspectives on flood management in the Rhine and Meuse rivers. *River Research and Applications*, *20*(3), 327–342. https://doi.org/10.1002/rra.782

Moreta, P. J. M., & Martin-Vide, J. P. (2010). Apparent friction coefficient in straight compound channels. *Journal of Hydraulic Research*, *48*(2), 169–177. https://doi.org/10.1080/00221681003704137

Myers, W. R. C. (1978). Momentum transfer in A compound channel. *Journal of Hydraulic Research*, *16*(2), 139–150. https://doi.org/10.1080/00221687809499626

Naghavi, M., Mohammadi, M., & Mahtabi, G. (2022). An experimental evaluation of the blocks in floodplain on hydraulic characteristics of flow in a meandering compound channel. *Journal of Hydrology*, *612*, 127976. https://doi.org/10.1016/j.jhydrol.2022.127976

Nagy, J., Kiss, T., Fehérváry, I., & Vaszkó, C. (2018). Changes in floodplain vegetation density and the impact of invasive Amorpha Fruticosa on flood conveyance. *Journal of Environmental Geography*, *11*(3–4), 3–12. https://doi.org/10.2478/jengeo-2018-0008

Nakashizuka, T. (2001). Species coexistence in temperate, mixed deciduous forests. *Trends in Ecology & Evolution*, *16*(4), 205–210. https://doi.org/10.1016/S0169-5347(01)02117-6

Nepf, H. M. (1999). Drag, turbulence, and diffusion in flow through emergent vegetation. *Water Resources Research*, *35*(2), 479–489. https://doi.org/10.1029/1998WR900069

Nepf, H. M. (2012). Flow and transport in regions with aquatic vegetation. *Annual Review of Fluid Mechanics*, *44*(1), 123–142. https://doi.org/10.1146/annurev-fluid-120710-101048

Nezu, I., Onitsuka, K., & Iketani, K. (1999). Coherent horizontal vortices in compound open channel flows. In *Hydraulic modeling: Proceedings of the International Conference on water, environment, ecology, socio-economics and health engineering* (pp. 17–32). Singh V, Seo I, Sonu J.

Ochs, K., Egger, G., Weber, A., Ferreira, T., Householder, J. E., & Schneider, M. (2020). The potential natural vegetation of large river floodplains – From dynamic to static equilibrium. *Journal of Hydro-Environment Research*, *30*, 71–81. https://doi.org/10.1016/j.jher.2020.01.005

Olde Venterink, H., Vermaat, J. E., Pronk, M., Wiegman, F., van der Lee, G. E. M., van den Hoorn, M. W., et al. (2006). Importance of sediment deposition and denitrification for nutrient retention in floodplain wetlands. *Applied Vegetation Science*, *9*(2), 163–174. https://doi.org/10.1111/j.1654-109X.2006.tb00665.x

Peltier, Y., Proust, S., Riviere, N., Paquier, A., & Shiono, K. (2013). Turbulent flows in straight compound open-channel with a transverse embankment on the floodplain. *Journal of Hydraulic Research*, *51*(4), 446–458. https://doi.org/10.1080/00221686.2013.796499

Peltier, Y., Rivière, N., Proust, S., Mignot, E., Paquier, A., & Shiono, K. (2013). Estimation of the error on the mean velocity and on the Reynolds stress due to a misoriented ADV probe in the horizontal plane: Case of experiments in a compound open-channel. *Flow Measurement and Instrumentation*, *34*, 34–41. https://doi.org/10.1016/j.flowmeasinst.2013.08.002

Phillips, J. D. (2009). Changes, perturbations, and responses in geomorphic systems. *Progress in Physical Geography: Earth and Environment*, *33*(1), 17–30. https://doi.org/10.1177/0309133309103889

Proust, S., Berni, C., & Nikora, V. (2022). Shallow mixing layers over hydraulically smooth bottom in a tilted open channel. *Journal of Fluid Mechanics*, *951*, A17. https://doi.org/10.1017/jfm.2022.818

Proust, S., Fernandes, J. N., Leal, J. B., Rivière, N., & Peltier, Y. (2017). Mixing layer and coherent structures in compound channel flows: Effects of transverse flow, velocity ratio, and vertical confinement. *Water Resources Research*, *53*(4), 3387–3406. https://doi.org/10.1002/2016WR019873

Proust, S., Fernandes, J. N., Peltier, Y., Leal, J. B., Riviere, N., & Cardoso, A. H. (2013). Turbulent non-uniform flows in straight compound open-channels. *Journal of Hydraulic Research*, *51*(6), 656–667. https://doi.org/10.1080/00221686.2013.818586

Proust, S., & Nikora, V. (2020). Compound open-channel flows: Effects of transverse currents on the flow structure. *Journal of Fluid Mechanics*, *885*, A24. https://doi.org/10.1017/jfm.2019.973

Ricardo, A. M., Franca, M. J., & Ferreira, R. M. L. (2016). Turbulent flows within random arrays of rigid and emergent cylinders with varying distribution. *Journal of Hydraulic Engineering*, *142*(9), 04016022. https://doi.org/10.1061/(ASCE)HY.1943-7900.0001151

Ricardo, A. M., Grigoriadis, D. G. E., & Ferreira, R. M. L. (2018). Numerical simulations of turbulent flows within an infinite array of randomly placed cylinders. *Journal of Fluids and Structures*, *80*, 245–261. https://doi.org/10.1016/j.jfluidstructs.2018.04.004

Ricardo, A. M., Koll, K., Franca, M. J., Schleiss, A. J., & Ferreira, R. M. L. (2014). The terms of turbulent kinetic energy budget within random arrays of emergent cylinders. *Water Resources Research*, *50*(5), 4131–4148. https://doi.org/10.1002/2013WR014596

Rominger, J. T., Lightbody, A. F., & Nepf, H. M. (2010). Effects of added vegetation on sand bar stability and stream hydrodynamics. *Journal of Hydraulic Engineering*, *136*(12), 994–1002. https://doi.org/10.1061/(ASCE)HY.1943-7900.0000215

Rominger, J. T., & Nepf, H. M. (2011). Flow adjustment and interior flow associated with a rectangular porous obstruction. *Journal of Fluid Mechanics*, *680*, 636–659. https://doi.org/10.1017/jfm.2011.199

Shiono, K., & Knight, D. W. (1991). Turbulent open-channel flows with variable depth across the channel. *Journal of Fluid Mechanics*, *222*, 617–646. https://doi.org/10.1017/S0022112091001246

Shiono, K., Scott, C. F., & Kearney, D. (2003). Predictions of solute transport in a compound channel using turbulence models. *Journal of Hydraulic Research*, *41*(3), 247–258. https://doi.org/10.1080/00221680309499970

Sokoray-Varga, B. (2022). *Inspection, post-processing and error filtering of measured velocity time series*. Bundesanstalt für Wasserbau (BAW). Retrieved from https://github.com/baw-de/Viper

Stocchino, A., & Brocchini, M. (2010). Horizontal mixing of quasi-uniform straight compound channel flows. *Journal of Fluid Mechanics*, *643*, 425–435. https://doi.org/10.1017/S0022112009992680

Straatsma, M. W. (2008). Quantitative mapping of hydrodynamic vegetation density of floodplain forests under leaf-off conditions using airborne laser scanning. *Photogrammetric Engineering & Remote Sensing*, *74*(8), 987–998. https://doi.org/10.14358/PERS.74.8.987

Sukhodolov, A. N., Schnauder, I., & Uijttewaal, W. S. J. (2010). Dynamics of shallow lateral shear layers: Experimental study in a river with a sandy bed. *Water Resources Research*, *46*(11), 1–18. https://doi.org/10.1029/2010WR009245

Sukhodolov, A. N., Sukhodolova, T. A., & Krick, J. (2017). Effects of vegetation on turbulent flow structure in Groyne fields. *Journal of Hydraulic Research*, *55*(1), 1–15. https://doi.org/10.1080/00221686.2016.1211183

Tjørve, E., & Tjørve, K. M. C. (2010). A unified approach to the Richards-model family for use in growth analyses: Why we need only two model forms. *Journal of Theoretical Biology*, *267*(3), 417–425. https://doi.org/10.1016/j.jtbi.2010.09.008

Tjørve, K. M. C., & Tjørve, E. (2017). The use of Gompertz models in growth analyses, and new Gompertz-model approach: An addition to the unified-Richards family. *PLoS One*, *12*(6), e0178691. https://doi.org/10.1371/journal.pone.0178691

Tominaga, A., & Nezu, I. (1991). Turbulent structure in compound open-channel flows. *Journal of Hydraulic Engineering*, *117*(1), 21–41. https://doi.org/10.1061/(ASCE)0733-9429(1991)117:1(21)

Trémolières, M., Carbiener, R., Eglin, I., Robach, F., Roeck, U., & Sanchez-Perez, J.-M. (1997). Surface water/groundwater/forest alluvial ecosystems: Functioning of interfaces. The case of the Rhine floodplain in Alsace (France). In F. Fournier, J. Mathieu, & J. Gibert (Eds.), *Groundwater/surface water ecotones: Biological and hydrological interactions and management options* (pp. 91–101). Cambridge University Press. https://doi.org/10.1017/CBO9780511753381.013

Trémolières, M., Sánchez-Pérez, J. M., Schnitzler, A., & Schmitt, D. (1998). Impact of river management history on the community structure, species composition and nutrient status in the Rhine alluvial hardwood forest. *Plant Ecology*, *135*(1), 59–78. https://doi.org/10.1023/A:1009756428824

Truong, S. H., & Uijttewaal, W. S. J. (2019). Transverse momentum exchange induced by large coherent structures in a vegetated compound channel. *Water Resources Research*, *55*(1), 589–612. https://doi.org/10.1029/2018WR023273

Truong, S. H., Uijttewaal, W. S. J., & Stive, M. J. F. (2019). Exchange processes induced by large horizontal coherent structures in floodplain vegetated channels. *Water Resources Research*, *55*(3), 2014–2032. https://doi.org/10.1029/2018WR022954

van Prooijen, B. C., Battjes, J. A., & Uijttewaal, W. S. J. (2005). Momentum exchange in straight uniform compound channel flow. *Journal of Hydraulic Engineering*, *131*(3), 175–183. https://doi.org/10.1061/(ASCE)0733-9429(2005)131:3(175)

Västilä, K., & Jilbert, T. (2025). Evaluating multiannual sedimentary nutrient retention in agricultural two-stage channels. *Scientific Reports*, *15*(1), 722. https://doi.org/10.1038/s41598-024-84956-2

Villada Arroyave, J. A., & Crosato, A. (2010). Effects of river floodplain lowering and vegetation cover. *Proceedings of the Institution of Civil Engineers—Water Management*, *163*(9), 457–467. https://doi.org/10.1680/wama.900023

Ward, J. V., Tockner, K., & Schiemer, F. (1999). Biodiversity of floodplain river ecosystems: Ecotones and connectivity. *River Research and Applications*, *15*(1–3), 125–139. https://doi.org/10.1002/(sici)1099-1646(199901/06)15:1/3<125::aid-rrr523>3.0.co;2-e

White, D. C., Morrison, R. R., & Nelson, P. A. (2023). Experimental observations of floodplain vegetation, bedforms, and sediment transport interactions in a meandering channel. *Journal of Geophysical Research: Earth Surface*, *128*(9), e2023JF007136. https://doi.org/10.1029/2023JF007136

Wittmann, F., Householder, J. E., Piedade, M. T. F., Schöngart, J., Demarchi, L. O., Quaresma, A. C., & Junk, W. J. (2022). A review of the ecological and biogeographic differences of Amazonian floodplain forests. *Water*, *14*(21), 3360. https://doi.org/10.3390/w14213360

Wittmann, F., Schöngart, J., & Junk, W. J. (2010). Phytogeography, species diversity, community structure and dynamics of central Amazonian floodplain forests. In W. J. Junk, M. T. F. Piedade, F. Wittmann, J. Schöngart, & P. Parolin (Eds.), *Amazonian floodplain forests* (Vol. 210, pp. 61–102). Springer Netherlands. https://doi.org/10.1007/978-90-481-8725-6_4

Wohl, E. (2021). An integrative conceptualization of floodplain storage. *Reviews of Geophysics*, *59*(2), e2020RG000724. https://doi.org/10.1029/2020RG000724

Xiao, Y., Liu, J., Wang, N., Gualtieri, C., Zhang, T., Liu, J., et al. (2022). Numerical simulation of overbank hyporheic transport and biogeochemical reactions in a compound channel. *Hydrological Processes*, *36*(8), e14670. https://doi.org/10.1002/hyp.14670

Xiao, Y., Wang, N., Liang, D., & Liu, J. (2018). Flow structures in trapezoidal compound channels with different side slopes of main channel. *International Journal of Civil Engineering*, *16*(7), 823–835. https://doi.org/10.1007/s40999-017-0212-9

Zhang, L., Zhang, S., & Huang, H. (2024). Study on the resistance characteristics of layered vegetation to overland flow. *Ecohydrology*, *17*(2), e2621. https://doi.org/10.1002/eco.2621